# Automated High Throughput Linear Actuator for Engineered Tissue

A Major Qualifying Project Report:
Submitted to the Faculty
of the
WORCESTER POLYTECHNIC INSTITUTE

In partial fulfillment of the requirements for the
Degree of Bachelor of Science

Submitted By:

Benjamin Chaffee

Thomas DiPersio

Katherine Kowalczyk

Victoria Velashea

Date: April 25, 2019

Approved:

Prof. Kristen L. Billiar, Advisor

# Table of Contents

# Table of Tables

# Table of Figures

# Acknowledgements

We would like to thank Professor Kristen Billiar and Ying Lei for all of the time and effort that they have put into this project. Without their support and knowledge this project would not have been possible. We would also like to thank Frank Benesch-Lee for giving us inspiration for our design.

# Abstract

Engineered tissue models are currently being investigated to gain a better understanding of the mechanobiology of skeletal tissue, as well as their potential role in drug research and development. Presently, there are many limitations and challenges associated with choosing materials that best mimic the complex mechanical properties found in native tissues. Current devices use mechanical and electrical actuation to stimulate engineered tissue scaffolds *in vitro* to improve and strengthen the mechanical properties of the constructs. Although these devices have proven successful in increasing cell alignment, myofiber size and cell proliferation, majority of these devices are expensive and lack highthorughput. Therefore, the purpose of this project is to aid and accelerate research in the field of mechanobiology and drug development, by developing a device that can effectively and efficiently actuate *in vitro* tissue scaffolds in order better observe and understand the effects of cyclic actuating has on improving the maturity rate and mechanical properties of engineered tissue constructs. The team accomplished this by designing a device to meet the needs of our clients. The final device has the ability to cyclically mechanically actuate scaffolds at varying strains and frequency while maintaining a sterile environment for the scaffolds to grow and mature. The device also allowed for the clients to accurately image the scaffolds, such that stress, strain and force applied on the constructs can be analyzed. The team conducted a variety of device verification tests to ensure client satisfaction, these included, a strain accuracy test, a camera accuracy test as well as a tissue test. Based on the results of the testing, the team was able to determine that the device met our client objectives. In the end, the device was able to perform multiple strains at 1 Hz with 5% accuracy, and take clear high resolution images that allowed for precise stress and strain calculations to be performed on realistic tissue constructs.

# Chapter 1: Introduction

The pharmaceutical industry in the United States is a multibillion dollar market focused on solving health and medical problems through drug research and development. In recent years, the pharmaceutical industry has seen a spike in the development and consumption of drugs, however there are still many ways to optimize and improve the process of drug development. One such way, is by using tissue engineered scaffolds to mimic *in vivo* like muscle conditions and responses, such that new drugs can be tested in an ethical and appropriate manner. In the case of clinical applications, engineered tissue models are currently being investigated to gain a better understanding of the mechanobiology of tissue as well as their use in drug develop (Tarum, 2017). There are currently many challenges and limitations associated with choosing materials that best mimic the complex and dynamic mechanical properties found in native tissues (Webber, 2015). Hence, there is a immediate and significant need for *in vitro* tissue models that allow for more accurate, intricate and complete drug development research. Tissues models that are best able to mimic the mechanical properties of native tissues will greatly impact the current method of drug development as it relates to cell to material integration as well as tissue integration.

The most challenging aspect of mimicking native muscle tissues is reproducing the maturity of native tissues. There are many significant properties of tissues that are essential to their function. Muscle fibers are composed of two main protein filaments, actin and myosin. These filaments form bands together to develop the sarcolemma. The sarcolemma shapes myofibrils which are responsible for muscle contraction (Theadom, 2014). Over time muscles fibers develop viscoelastic properties from sustained tension and relaxation. In addition, mature tissues often exhibit increase cell alignment and proliferation, increased cell to cell and cell to extracellular matrix regulation, and larger myotube and myofiber diameter (Ahadian, 2013; Powell, 2002; Grossia, 2007) . All of these characteristics allow the tissue to function and grow properly and are responsible for the chemical and mechanical responses in the body. Therefore, for clinical research purposes it is essential to be able to recreate similar mechanical strains and stresses that native tissues experience, in order to obtain accurate responses and data to new and developing drugs.

The current methods to stimulate engineered tissue models *in vitro* include mechanical, electrical and magnetic stimulation. All of these techniques provide a specific type of stimulation or actuation that applies a stress and strain on the tissue model. Current research suggests that these applied strains will strengthen the tissue models and improve the physical and biological properties of the tissue (Powell, 2002). Such as, increased cell differentiation and proliferation, improved myofiber organization and alignment as well as an increased extracellular matrix (Theadom, 2014). In addition, it has been proven

that the effect of cyclic loading can drastically improve the overall strain and contraction ability of the engineered tissue models to best mimic similar properties in that of native tissues (Rose, 2004).

Despite the many clinical advantages of engineered tissue scaffolds, there is still a lot of work being done surrounding the best way to most effectively mature and stimulate them. In addition, there are many areas including the maturation process and the mechanical properties of tissues both *in vitro* and *in vivo* that are still being investigated and further understood. Although there are a few current linear actuators and bioreactors that accomplish the goal of maturing in *vitro* tissue constructs, these devices are often not for commercial use, extremely expensive and not high throughput. Therefore, the purpose of this project is to design a relatively inexpensive high throughput device that can be used to actuate and mature in vitro tissue scaffolds effectively and efficiently, while also allowing for proper imaging. The ability to accurately image the tissues is a significant aspect of this project in order to observe the effects of actuation on the tissue models as well as correctly measure and calculate the mechanical properties of the scaffolds. The optical imaging in conjunction with the high throughput actuation of the tissue models will help progress advancements being made in mechanobiology as well as drug development and drug discovery. The following report, outlines the process the team took to producing the final design and highlights specific design choices the team made.

# Chapter 2: Background

## 2.1 Purpose of Project

Our project is focused on researching the benefits that a mechanical actuation device would have on engineered tissue scaffolds and developing a device to achieve these benefits. This can help to aid and accelerate research in the field of mechanobiology and drug development, by better understanding the effect actuating engineered tissues has on improving their maturity rate and mechanical properties. To accomplish this, our team must first understand modern day practices in the field. Currently, the objective of tissue engineering is to use living cells as engineering materials to grow biological substitutes that repair, replace, restore, and improve the functions of diseased or damaged tissue (Neuenschwander, 2004; Eisenbarth, 2007). Much of the literature that is currently being done on stretching engineered tissue is focused on skeletal muscle tissue.

## 2.2 Muscle Tissue Anatomy in Vivo

The natural characteristics of skeletal tissues play a huge role in the ability for the tissue to function and work properly. Therefore, it is extremely important to understand the anatomy of muscle tissues to better understand the properties needed for our *in vitro* models.

### *2.2.1 Form and Function*

Skeletal muscles are formed in many shapes and sizes, depending on what the exact functions of the skeletal muscle will be. Every muscle in the body is made up of hundreds or thousands of muscle cells, also known as a muscle fiber, that attach together to make a skeletal muscle. The bundle of muscle fibers that form one muscle are covered with connective tissue called epimysium. The epimysium is then covered by fascia, another layer of connective tissue, to separate the different bundles of muscle fibers. Within each muscle the fibers are split up into smaller sections of muscle fibers, called perimysium. Blood vessels and nerves run in between perimysium within the muscle. The muscle anatomy can be seen below in Figure 1, showing how the muscle fibers and connective tissue form one muscle (SEER, 2018).

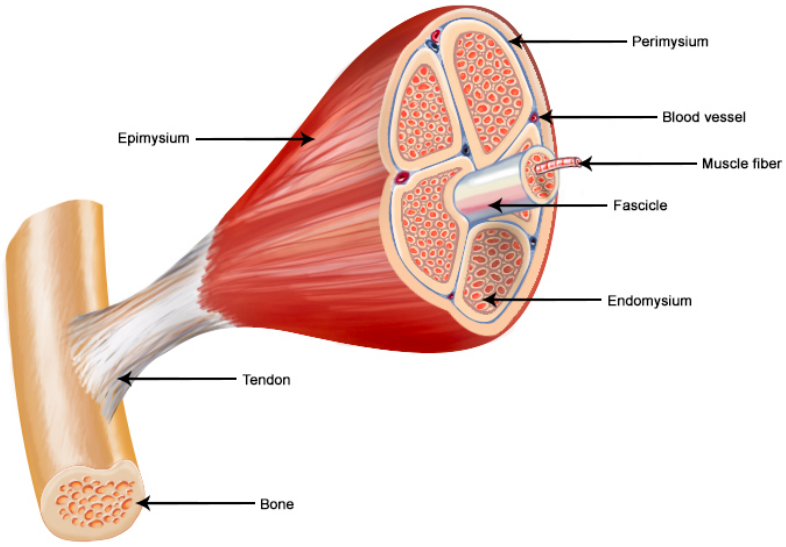


**Figure 1: Anatomy of Muscle**

Shown here is the anatomy of muscle. Within muscles are bundled fascicles containing muscle fibers. These muscle fibers are composed of muscle tissue such as that which we will be investigating in our research.

Muscles are then attached to bones. Each end of the muscle is attached by a tendon. The tendon attaches to the bone, which connects the muscle to the bone. Muscles connect two bones together at a joint, and help to stabilize that joint. Having the muscle connected to two seperate bones allows for movement. When the muscle contracts it moves one of the bones, while the other bone remain stationary. The movement of one of the bones in respect to the other bone it is attached to allows for movement of the body. Movement is one of the main functions of muscles. Muscles also allow the body to pick up weights, maintain our posture and generate heat when the body is doing an activity. Muscles perform their functions from impulses from nerves that run through the muscle. When the nerve sends an impulse to the muscle it causes the muscle to contract, causing movement in the body. When the impulse is removed the muscle will relax (SEER, 2018).

### *2.2.2 Development*

Muscles are formed through a process called myogenesis. Myoblasts produce rapidly in response to the presence of fibroblast growth factors. Myoblasts can form together to make multinucleated cells called myotubes. Once the myotubes are formed they align with other myotubes that are surrounding it and fuse together. Skeletal muscle cells are long, cylindrical cells. When hundreds or thousands of muscle cells align together they form a singular muscle. In the case that myoblasts do not fuse to make myotubes, they dedifferentiate back into myosatellite cells. Myosatellite cells have the ability to differentiate into any type of muscle cells (SEER, 2018).

### *2.2.3 Physical Properties*

There are four main mechanical properties of skeletal muscle cells. The four properties include contractility, elasticity, extensibility and excitability (Gennisson, 2010). Contractility refers to how fast and hard the muscle contracts in response to a stimulus that is applied. Since a singular muscle is comprised of many different muscle fibers, how well all of the fibers contract together will determine how the muscle as a whole will contract. When a muscle contracts and relaxes it changes its length. Skeletal muscles need to contract and relax without damaging the muscle. This refers to the elasticity of the muscle. Over time the original size of the muscle should not significantly change. The ability for skeletal muscle cells to stretch through contractions refers to their extensibility. Excitability is how the muscle cells can receive electrical impulses from nerves. How excited the muscle cell gets refers to how the muscle cell responds to the action potential from the nerve cell (Crystal, 2018).

## 2.3 Engineered Muscle Tissue in Vitro

### *2.3.1 Growth Process*

There are numerous ways to grow engineered tissue constructs, one current method to grow muscle tissue, practiced in the Billiar lab at Worcester Polytechnic Institutes Biomedical labs, is to form constructs by seeding the tissue across silicone posts within a 96-well plate. In order to do this, silicone posts are first molded outside of the well plate. The silicone posts are composed of two posts with an exaggerated head on each post, both connected to a shared base. Once molded, the posts are glued into place in the wells by hand. Following the placement of silicone posts inside the wells, the well and posts are sterilized using a 1% Pluronic treatment flood. Subsequent to the sterilization is the casting of a NIPAM gel within the well. This forms a platform for the next step, which is the casting of the tissue construct on top of the NIPAM. Because of the NIPAM, the tissue construct forms around the previously mentioned exaggerated heads at the top of the silicone posts. The construct is then left overnight to compact around the silicone posts after which the NIPAM solution is removed from the well. The end result is a compacted muscle tissue construct connecting the tops of the two silicone posts (Luciano thesis presentation).

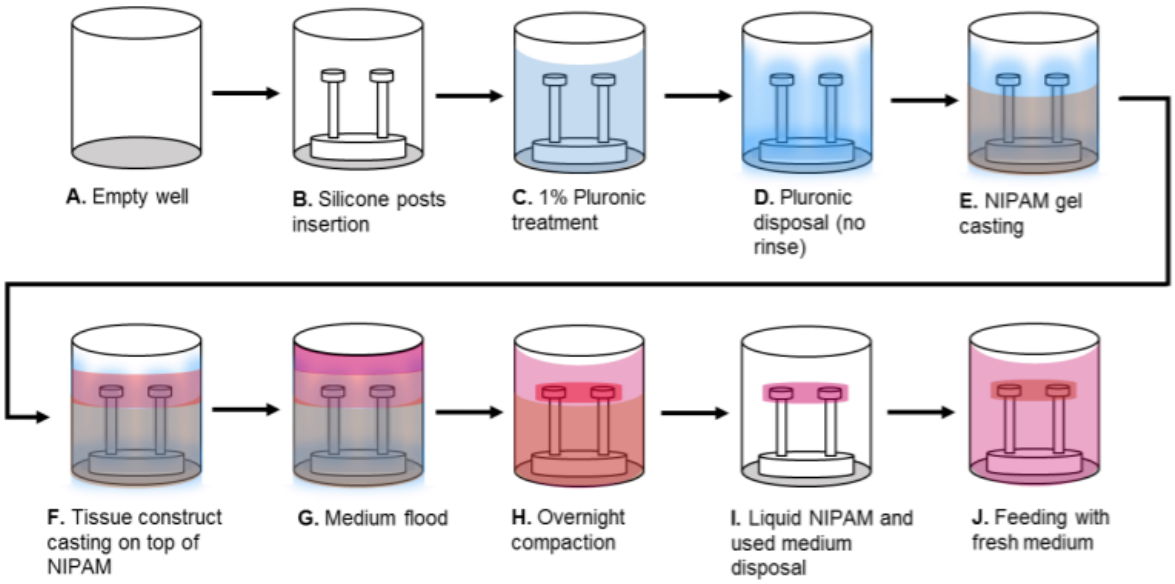


**Figure 2: Growth Process of Tissue**

Growth Process of Muscle Tissue Scaffolds. Silicone posts are glued into an empty well and treated with 1% Pluronic liquid, then a NIPAM gel is casted into the wells. The tissue construct is then formed on top of the NIPAM. A growth factor is then placed on top of the construct and left overnight to compact. Lastly, the medium and NIPAM is removed and new fresh medium is inserted. (Luciano thesis presentation)

In designing the posts, careful consideration was paid to the material used. Polydimethylsiloxane (PDMS), a silicone compound, was selected. PDMS is hydrophobic and also prevents infiltration of glycerol, methanol, or ethanol. These protective properties make PDMS suitable for the chemical treatments used to sterilize the posts as well as reusing the posts for tissue construct growths. Additionally, the material is biocompatible, making it further suitable for tissue construct growths. While not necessary, PDMS is also a transparent material, allowing for better visibility of the tissue growth process. Once the muscle tissue growth starts as well as when molding with the material, PDMS' deformable nature becomes advantageous. In the case of actuated posts, this will become especially beneficial. In addition to material properties, PDMS is inexpensive and thus lends itself to high-throughput applications (PDMS, 2018).

The supporting material used is NIPAM, belonging to a family of environmentally sensitive polymers. Based on external stimuli such as temperature or pH levels, the polymers undergo change from a hydrophilic state to a hydrophobic state. Additionally, there can be an associated swelling or shrinking of the polymer as it undergoes these changes. The polymer's transition to a hydrophobic state eases in the process of removing the NIPAM from the well without disturbing the newly formed tissue construct (NIPAM, 2018)

### *2.3.2 Maturation Process*

Biomimicry is necessary for *in vitro* muscle tissues to be valuable in any tissue engineering applications. During *in vivo* muscle tissue growth, there are a number of external factors and internal characteristics that must be present for healthy muscle tissue to grow.

*In vivo,* muscle tissue is grown under precise conditions including the temperature, $CO_2$ content, and humidity. To best replicate this in laboratory settings, researchers typically incubate their systems while controlling these parameters. Temperature will be maintained at roughly 37°C , $CO_2$ levels will be maintained at roughly 5%, and humidity will be maintained at roughly 95%. To further simulate actual tissue growth in the lab, a number of growth factors and hormones are contained in a supplied medium. Primarily, the mixed medium contained neurobasal and NBactiv4. In past experiments, this medium has been present for 4 days before progressing with the experiment (Das, 2009; Hollander, 2006).

In addition to the conditions the tissue grows within, there a number of physiological checkpoints that occur during muscle tissue maturation. More specifically, these are sarcomere organization, clustering of Ryanodine, and the transition of myosin heavy chains (MHCs). Sarcomeres are the functional units of contraction within the muscle. They are a clustering of unidirectional myofilaments. Ryanodine is a molecule that functions to release calcium in the sarcoplasmic reticulum. Functionally speaking, it aids in the development of skeletal muscle by increasing the size of muscle cell groups as well as developing and organizing the tissue. Furthermore, a sign of skeletal muscle development is the transition of MHCs, the motor proteins of muscle tissues, from an embryonic isoform to a neonatal isoform (Wells, 1996).

### *2.3.3 Physical Properties*

In determining the maturity of the muscle tissue, there are several factors to be measured or observed. In similar projects in the past, researchers have observed properties such as mean myofiber diameter, myofiber density, passive force properties, and viscoelastic properties of the tissue (Powell, 2002). Additionally, our project would aim to measure the applied strain to the tissue. The reasoning for measuring applied strain is that a correlation between applied strain and force measured could be found and used to evaluate viscoelastic properties of the muscle tissue. These measured properties can be categorized as those which are visually measurable, such as myofiber diameter and myofiber density, and those which are measurable with the aid of a force gage, such as passive force properties and viscoelastic properties (Shimoyama, 2010).

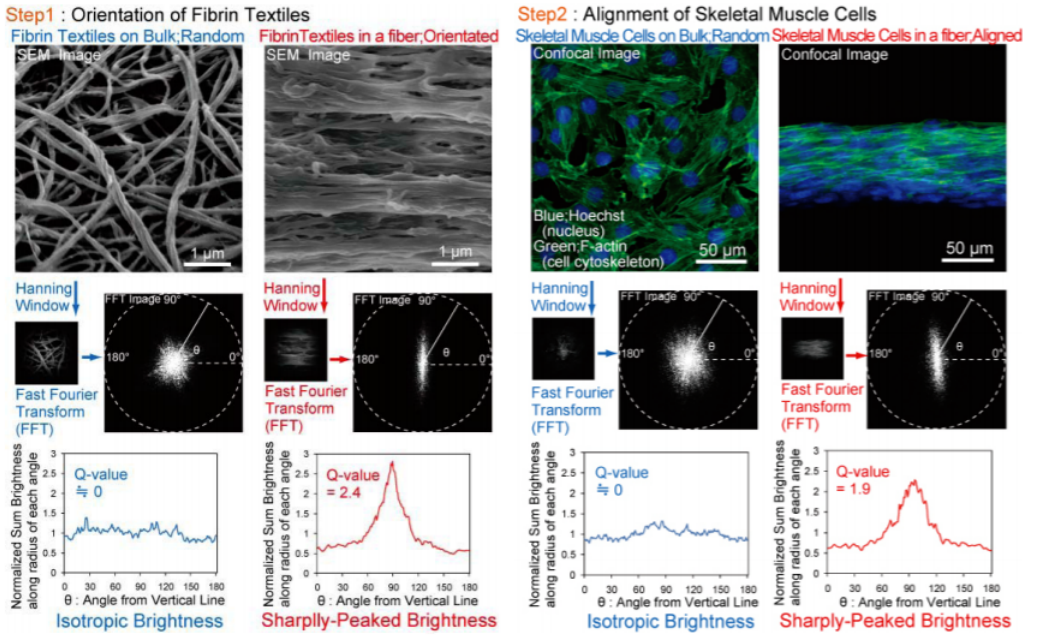


*Fig.3: Textiles of fibrin hydrogel of SEM images and Quantitative evaluation of Fast Fourier Transform (FFT) of the images; Bulk and Fiber. Q-Value was defined as $\omega/\Delta\omega$, $\omega$ is maximum value of vertical axis, $\Delta\omega$ is half width. Textiles of fibrin are orientated and FFT image indicates sharply-peaked brightness.*

*Fig.4: Skeletal muscle cells of skeletal muscle cells of confocal images and quantitative evaluation of Fast Fourier Transform (FFT) of the images; Bulk and Fiber. The skeletal muscle cells on fibrin hydrogel bulk grew randomly. On the other hand, the skeletal muscle cells in a fibrin hydrogel fiber grew aligned.*

**Figure 3: Alignment of Muscle Tissue**

This figure looks at the alignment of cells in multiple tissues. Focusing on both fibrin and skeletal muscle samples, the figure compares randomly aligned tissue with highly aligned tissue. Researchers from the University of Tokyo quantified these images using a Fast Fourier Transform. This analysis shows the angle of each fiber in the picture, with aligned tissue falling generally along the same angle (Shimoyama, 2010).

The visually measurable properties focus on the myofibers present. Namely, researchers will record myofiber alignment, mean myofiber diameter, and myofiber density within a sample (Shimoyama, 2010; Close, 1972). Myofiber alignment is investigated as the alignment of fibers is critical to the strength of the muscle tissue. A highly aligned tissue sample is able to longitudinally distribute applied stress throughout the tissue as well as even contractile forces. In the case of randomly aligned fibers, the tissue is unable to deliver full contractile force in any one direction. Figure 5 shows how researchers will measure the orientation of muscle fibers. The images, taken with a scanning electron microscope or a confocal image of dyed fibers, each show an example of randomly aligned fibers and aligned fibers. Using a fast Fourier Transform, researchers were able to analyze the images and determine the average angle of the fibers and as a result, the degree of alignment. Similarly, the mean myofiber diameter and myofiber density can be found using image processing techniques (Shimoyama, 2010).

To measure passive force properties and viscoelastic properties, a force transducer is typically used. Compared to the visually measured properties mentioned prior, this tactic is much more

straightforward. A force transducer is mounted in series with the actuating motor delivering strain to the tissue and as a result, a force measurement is obtained. To differentiate between passive force properties and viscoelastic, measurements are taken both when there is no force being applied to the tissue and when there is force being applied to the tissue. Respectively, this supplies measurements on passive force created and viscoelastic force created (Madden, 2015).

## 2.4 State of the Art Stimulation of Engineered Muscle Tissue in Vitro

There are a variety of different processes and methods used to precondition and stimulate in vitro engineered muscles. Many of these methods involve a type of stimulation to accurately and precisely achieve the proper function and maturity found in native tissue models. The most common techniques are mechanical stimulation, magnetic stimulation, and electrical stimulation.

The positive effects of electrical exercise inside the body has long been understood and observed. Inside the body, electrical pulses known as action potentials trigger the central nervous system, causing the muscles to contract and tighten. Due to the this contraction and relaxation, normal healthy muscle tissues have extremely distinct characteristics, such as alignment and strength (Ahadian, 2013). One study correlated the maturity of myotubes with electrical stimulation in muscle cells, when compared to non stimulated myotubes. This included increased cell alignment and organization (Tarum, 2017). Given the benefits of naturally stimulated tissues, researchers have been exploring various methods to mimic these results in vitro tissue constructs to better mimic the properties found in the body. Table 1 below displays a small subset of current and past methods that have been used to research the effects of electrical and mechanical stimulation on in vitro tissue constructs.

**Table 1: Summary of the Benefits of Electrical and Mechanical Stimulation Methods**

| Type of Stimulation | Benefits of Stimulation in Vivo | Reference |
|---|---|---|
| Electrical | Regulate cell to cell and cell to extracellular matrix, this can enhance alignment and differentiation | Ahadian, 2013 |
| Electrical Pulse | Increased mayotube size and formation of striated sarcomeric structures | Tarum, 2017 |
| Electrical Pulse | Proteins such as activated protein kinase were released during contraction | Manabe, 2016 |
| Mechanical Strain | Improved unidirectional alignment and contractile forces. | Moon, 2008 |

| | | |
|---|---|---|
| Mechanical Force | Increased myofiber diameter, elasticity and applied force | Powell, 2002 |
| Mechanical Loading | Increased myoblast proliferation, differentiation and fusion | Grossia, 2007 |
| Electrical | Improved cell differentiation and alignment | Bursac, 1999 |
| Electrical | Increased cell expression | Dennis, 2000 |
| Electrical | Increased activation of signalling pathways as well as improved oxidation | Nikolić, 2016 |
| Mechanical | Improved cell activities such as proliferation, growth and migration | Kamble, 2016 |

### *2.4.1 Mechanical Stimulation*

Based on the sheer amount of current and past literature focused electrical and mechanical stimulation in vitro it is impossible to summarize all of the different test methods and procedures, however this section aims to highlight a few of the techniques of actuation.

Mechanical stimulation of engineered tissues has proven to improve the mechanical properties of tissue scaffolds to best mimic their native constructs. Uniaxial cyclic stretching can help improve these properties such as, fiber alignment, elongation, elastic modulus thickness and strength (D'Amore, 2016). Oftentimes, mechanical actuation of *in vitro* muscles tissues is measured by applied stress and strain. Strain is calculated by the change in length of the specimen, while stress relates to the applied force. Repeated and gradual cycling of elongation and strain in engineered tissue constructs lead to an improvement of mechanical and physical properties (Moon, 2008).

One example of mechanical actuation of in vitro tissue specimens was conducted by W. Merryman. He and his team designed a bioreactor step motor system as shown in Figure 4 (Merryman, 2007).

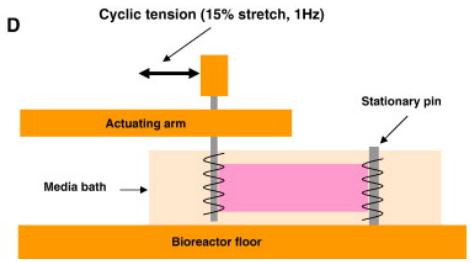


**Figure 4: Mechanical Actuation by Step Motor**

Mechanical Actuation by Bioreactor Step Motor System. This system uses an actuating arm attached to a tension bioreactor. The tissue construct is formed around a stationary pin and the actuating arm in medium. The bioreactor applies a 15% tensile stretch at 1Hz to the tissue construct (Merryman, 2007).

This design consisted of a four by two plate, such that a total of eight tissue specimens could be mechanical stimulated simultaneously at the same strain. For the purposes of their design the actuating arm was connected to a motor driven linear actuator that could stretch up to 15% of the strain. The motor was set to move a specific distance that corresponded to the set strain. As the actuating would move the attached pin would also move effectively stretching the specimen away form the stationary pin. In this experiment, the tissue models were stretched 15% at 1Hz.

Although this experiment proved successful for the purpose of their area of interest, this system does not exhibit a functional way to apply varying strains within the plate. According to the article, this experiment only tested a tension group and null group and did not vary strains or progressively increase strains. Despite this, the experiment concluded that tension improved tissue maturation when compared to the non mechanically stimulated group (Merryman, 2007).

Another example of mechanical actuation is shown in Figure 5, this device applied uniaxial tension to eight specimens simultaneously using a linear actuator. The experiment was conducted over four group in a 21 day timeline. The four groups, were comprised of a control group that did not receive a strain, a 15% strain group, a 30% strain group and a 30% strain group all at a frequency of 1Hz. Mechanical actuation at a 30% cyclic strain showed the greatest proliferation of cells and the collagen matrix. Over stimulation of the 50% strain group displayed a decrease in fiber alignment and self assembly due to excess ruptures (D'Amore, 2016).

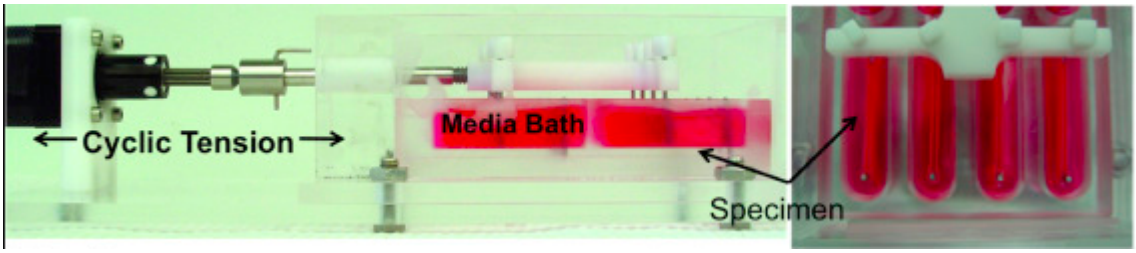


**Figure 5: Mechanical Actuation by Linear Actuator**

Mechanical Actuation by Linear Actuator. Tissue constructs are grown around one stationary pin and one actuating pin. The actuating pins are attached to a linear actuator that applies cyclic tension to the tissue constructs (D'Amore, 2016).

Another type of mechanical actuation is pressure actuation, also known as pneumatic actuation. In pneumatically actuated muscle tissue setups, an air pressure differential is used to cause strain on the muscle tissue (Kamble, 2012; Shimizu, 2012; Watanabe, 2005) . This can be done in a variety of ways utilizing either positive or negative pressure. Typically, the process involves deformation of a membrane

that cells or tissues are cultured directly onto. One of the first instances of this form of actuation was by Kamble *et al,* he and his team's design is shown below in Figure 6.

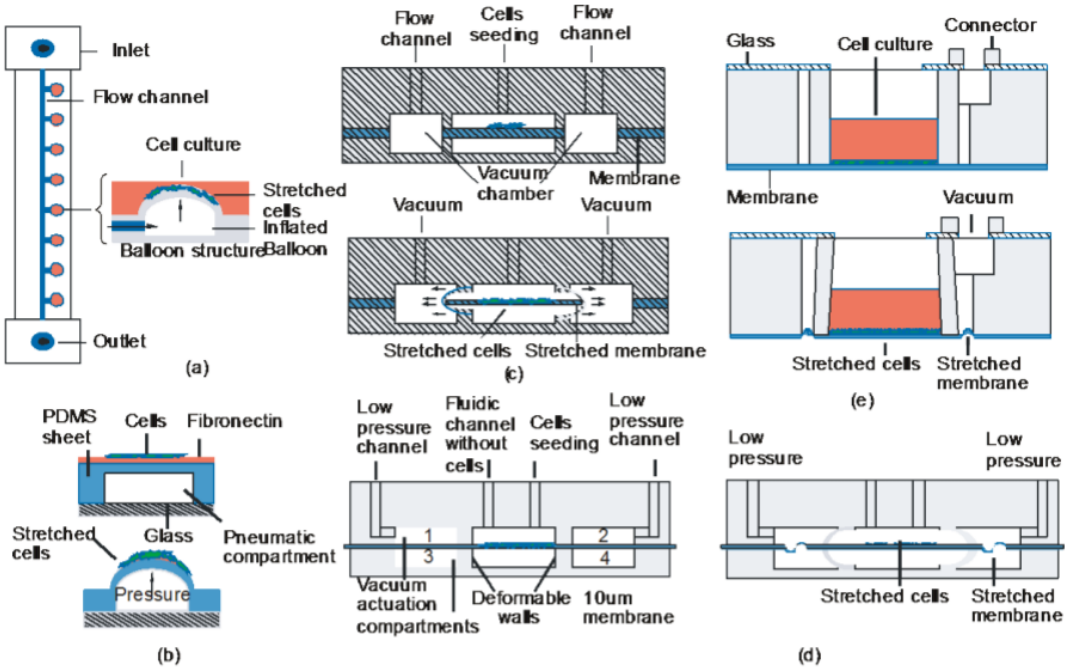


**Figure 6: Pneumatic Actuation of Tissue**

This figure provides a variety of methods for actuating muscle tissue via pneumatic means. Generally, the designs work on the principle of air pressure, positive or negative, causing strain on a flexible membrane that is in turn applied to the tissue (Kamble, 2012).

Shimizu utilized positive air pressure to inflate a series of connected balloons. As the ballooning membrane was inflated, the membrane began to stretch and the tissue constructs attached to the membrane experienced strain as well (Fig 6a) (Kamble, 2012). Additionally, pneumatic actuation can be caused by negative pressure as well, as in Huang and Nguyen's work (Nguyen, 2002). Their research led to a fixture in which a vacuum source on either side of the connected membrane led to the embrane being uniformly stretched in both directions (Fig 6c).

Pneumatic actuation presents several advantages over other actuation methods. Namely, it is a relatively easy setup, it provides uniform strain, and there is no direct contact with tissues, aiding in both sterility and measurement (Watanabe, 2005). Generally speaking, pneumatically actuated systems incorporate a deformable membrane, a fixture to which the deformable membrane is fastened, and a void between the two that can be inflated or deflated. Compared to other methods of actuation, there can be a low number of moving parts in this setup. In terms of applied strain, so long as the membrane is made uniformly, there will be an equal strain applied to the tissue throughout the setup. This is helpful in

finding repeatable processes for experiments. As the tissue is always being strained by the membrane and never directly by an applied force, there is no direct contact in pneumatic actuation setups. For maintaining a sterile environment for the tissues, this is vastly beneficial. Furthermore, the lack of direct contact allows for the tissues to be more easily observed as there are no obstructions.

While pneumatic actuation prevents several strong advantages over other actuation methods, it can present difficulties in measuring resultant forces of actuation. In direct mechanical actuation, the force applied by the system and delivered back to the system by the muscle tissue can be easily and directly measured using a force gage. In the case of pneumatic actuation, the force applied to the membrane can often be found very easily, but this will sometimes not be a direct relation to the strain applied to the tissue connected to the membrane.

### *2.4.2 Magnetic Stimulation*

Magnetic Stimulation was originally developed to stimulate peripheral and central nerves, but more recently has made its way into the field of skeletal muscle. Magnetic stimulation has been used on human muscles to induce effortless muscle fatigue and training in the quadriceps and pelvis, and has even treated urinary incontinence in women. Overall magnetic stimulation is able to induce muscle twitch, for this reason it has been investigated as therapeutic method for skeletal muscle diseases.

A study was conducted to investigate muscle injury and magnetic stimulation *in vivo*. This study was performed on mice with leg injuries; the study's results showed that magnetic stimulation does not harm muscles but actual improves muscle regeneration (Stolting, 2016). The magnetic stimulation minimized the inflammatory infiltrate and formation of muscle scar after trauma was experienced. Although this study showed promise for magnetic stimulation in muscle regeneration, our team has a focus of magnetic stimulation *in vitro*.

A study performed was performed in which researchers used an approach of using magnetic actuation to enable mechanical stimulation of microtissues. The design is shown below in Figure 7. In the wells, pairs of flexible pillars (PDMS substrate) are exposed to a mixture of cells and extracellular matrix to form a microtissue suspended between the pillars. One of the pillars in each well had a Ni microsphere bonded to it. A small Ni bar was placed close to the magnetic pillar of the well. Next, in the figure represents the externally applied magnetic field which creates the magnetic force between the sphere and bar indicated by $\mathbf{F}_{Mag}$ in the figure. The deflection of the pillar that does not have the Ni sphere provides the readout of the applied force of the system (Xu, 2015).

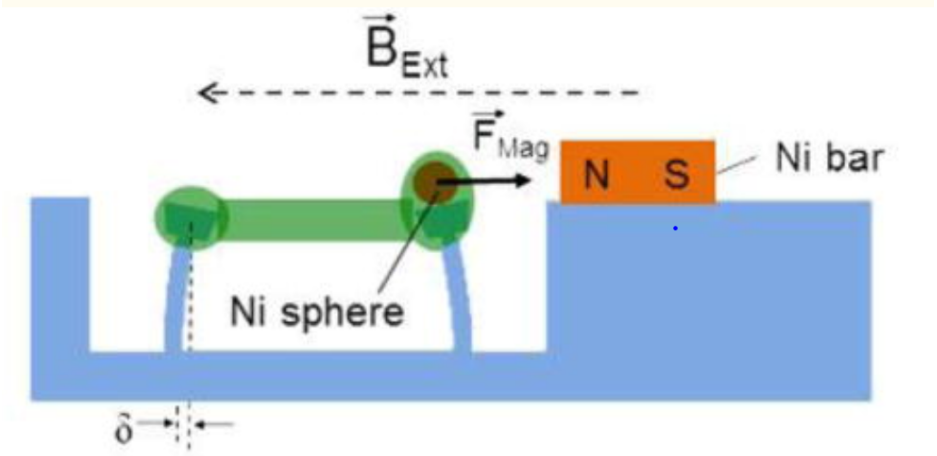


**Figure 7: Magnetic Actuation of Tissues**

Magnetic Actuation of Microtissues. The figure demonstrates how the Ni sphere is pulled by the magnetic force towards the Ni bar. The microtissue is stretched between the two silicone pillars by the force generated magnetically. The displacement of the pillar on the left in the figure was used to calculate the applied force of the system (Xu, 2015).

This system was able to generate forces sufficient to stretch the microtissues by 3%. Using sequential imaging, the stress and strain of the group of microtissues was able to be recorded. This case of magnetic actuation was a success to these researchers since they were able to reliably record elastic modulus and other quasi-static mechanical properties of the microtissues. Although, the data set they were able to successfully record was only for 7 microtissues.

### *2.4.3 Electrical Stimulation*

In vivo skeletal muscles are generally electrically stimulated by the beating of the heart and through electrical impulses from nerves through mature skeletal muscles (Rangarajan, 2013). By stimulating skeletal cells electrically it can help to align the muscle fibers, increase the size of the skeletal muscle fibers, increase the force that a muscle can generate and can increase the expression of contractile proteins. Electrical stimulation has shown to be beneficial to skeletal muscle cells in vitro (Rivera, 2012).

In order to electrically stimulate muscle fibers in vitro electrodes need to be placed inside of the medium that the muscle fibers that growing within. The electrodes do not need to be puncturing the muscle fibers, as long as they are inserted into the medium that the muscle fibers are growing in then it will be able to electrically stimulate the muscle fiber. In the example below in Figure 8, stainless steel electrodes are used (Martinez, 2010).

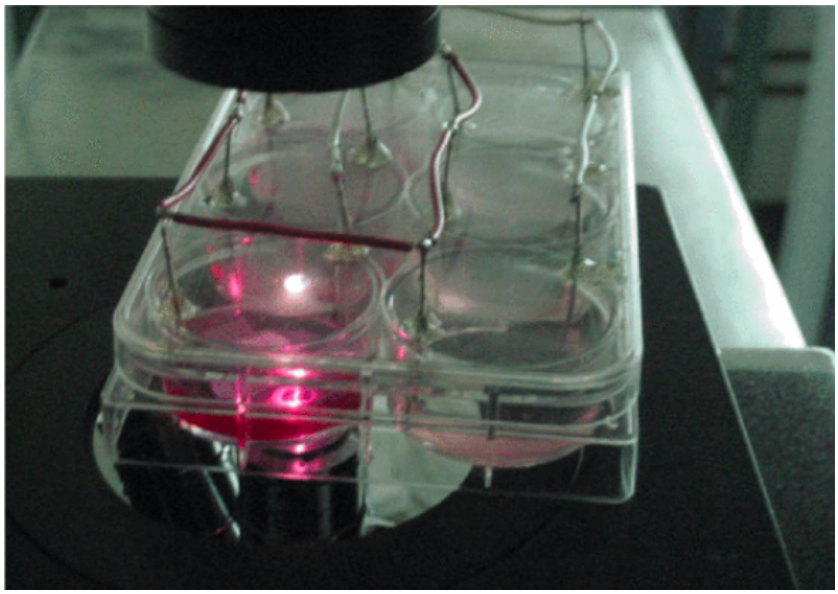

**Figure 8: Electrical Stimulation of Tissues**

This figure provides an example of electrical stimulation acting on muscle cells. In this case, stainless-steel electrodes create an electric field across the tissue sample. This field actuates the tissue similarly to the process found in vivo (Martinez, 2010).

In this example two stainless steel electrodes are placed on either side of a petri dish to stimulate different skeletal muscle cells. This experiment was done at multiple frequencies, 200 Hz, 10 Hz and 3.33 Hz. The pulse amplitude that was applied was also changed between 400 mVpp and 150 mVpp (Martinez, 2010). There are many different factors that are considered when electrically stimulating a muscle fiber. When stimulating the muscle fibers electrically the frequency, pulse width and pulse amplitude can affect how the muscle will react to stimulation. Exact frequencies, pulse widths, pulse amplitude and duration of electrical simulation has not been scientifically determined when growing muscle fibers in vitro, but is most successful when it closely mimics the parameters that are seen within the body. One study compared different voltage pulses, frequencies and durations and how it affected the outcome of the muscle cells. The results can be seen in Table 2 below (Rangarajan, 2013).

**Table 2: Comparison of Electrical Stimulation Factors on Muscle Cells**

| Cell source | Cyclic regime | Duration | Outcome | References |
|---|---|---|---|---|
| NRCMs | 2 ms pulses 5 V/cm, 1 Hz | 8 days | Improved CM ultrastructure, alignment, contraction, excitability | Radisic *et al.* 106 |
| NRCMs | 2 ms pulses 4 V/cm, 1 Hz | 9 days | Increased CM volume fraction, elongation, connexin-43 expression | Lasher *et al.* 75 |
| Human ESC-CMs | 2.5 V/cm, 1 Hz | 14 days | Enhanced CM sarcomerogenesis, Ca handling, electrical properties | Lieu *et al.* 79 |
| Human ESC/iPSC-CMs | 3–4 V/cm, 1–6 Hz for 7 days, then 1 Hz | 7–21 days | Promoted cell organization, conduction velocity, $Ca^{2+}$ handling | Nunes *et al.* 95 |
| C2C12 line | 5 V/cm, 1 Hz for 1 h every 6 h | 7 days | Enhanced formation of striations, contractile protein expression | Liao *et al.* 77 |
| C2C12 line | 12.5, 25, 50 V/cm, 4 pulses at 10 or 100 Hz, then 3.6 s rest | 7 days | Higher pulse amplitude increased force production and excitability, higher pulse frequency increased the rate of protein synthesis | Donnelly *et al.* 40 |

There are no set industry standards for what parameters should be used when electrically stimulating a cell. Most parameters are set through different experiments. Electrical stimulation on its own helps to mature cells faster and can help make muscle fibers that are grown in vitro more closely mimic muscle fibers that are grown in vivo. Cyclic electrical stimulation has been shown to beneficial to the maturity and differentiation of muscle fibers. Combining electrical stimulation with other forms of stimulation, like mechanical stimulation, can even further improve the way muscle fibers are grown in vitro.

# Chapter 3: Project Strategy

## 3.1 Initial Client Statement

Currently, muscle tissue is cultured across flexible silicone posts fixed inside of wells. The flexible silicone posts are glued to the bottom of the wells after they have been molded to create a biocompatible surface for the tissue to grow across. The posts have been designed such that as the tissue grows under tension, it is held in place by the ball-end of the silicone posts. While this design allows for tissue growth, there is currently no way to actuate the muscle tissue. Actuation of the growing muscle tissue matures the tissue and in turn creates better lab models of muscle tissue that would be found in the body. Furthermore, the current system does not have a high throughput way to measure the strain and force being applied to the tissue. These measurements are critical to understanding the mechanical properties of the tissue.

To fulfill the client's requirements, the team will be designing a high throughput system for both actuation of the muscle tissue and measurement of the strain and force applied to the tissue. This design will not necessarily include a redesign of the silicone posts, however considering the design constraints presented by the silicone posts, it is likely that there will be a new post designed.

## 3.2 Revised Client Statement

The client is requesting a high-throughput system for actuating *in vitro* muscle tissue and measuring the force applied to the tissue. The system must apply a maximum of at least a 10% strain to the tissue at a frequency of 0.2-2 Hz. The system must be capable of actuating a minimum of eight tissue constructs at a time. Under normal operating conditions, this system must last for the course of one week. While this describes normal operating conditions, the system must be capable of progressive overload of the tissue with variable strains and frequencies. In addition to the described mechanical stimulation, the system must also be capable of applying variable electrical stimulation to each muscle tissue construct. Following the actuation, each individual tissue construct will be observed for myofiber diameter, myofiber density, passive force properties, and viscoelastic properties.

In designing the system, the team must consider the constraints associated. The budget for this system is $1,000, established by the $250 allotted to each team member. The environment in which the tissue constructs grow and are actuated must be completely sterile. The posts and wells that house the muscle tissues must be biocompatible. The system must all fit within an incubator that will maintain a desired temperature, $CO_2$ level, and humidity. The project must be completed within the 2018-2019 school year.

## 3.2 Design Requirements

This section outlines the design objectives and constraints of our project based on client feedback and input. Therefore, the device must meet the following requirements.

### *3.2.1 Design Objective*

After reviewing the initial client statement, researching the limitations and successes of similar projects and interviewing the client the team came up with the following objectives for our own design. The list of objectives are below in Table 3.

**Table 3: List of Design Objectives**

| **Design Objective** | **Specification of Objective** |
|---|---|
| Mechanical and Electrical Stimulation | Has the ability to stimulate the cell multiple ways |
| Strain | 2%, 5%, and 10% strain |
| Incremental strain over time | Be able to be stretched more over time |
| Frequency | 1 Hz |
| Duration | One week |
| High throughput | 96 wells |
| Measure stiffness of the tissue | Stretch and hold to desired strain while measuring post and tissue deformation |
| Repeatable and reproducible | Measured strain will be within 5% of the desired strain on a trial of at least 10 wells |

As discussed in our background, research has shown that by stretching cells while they are growing will cause them to be stronger and more mature faster than without actuating the tissue. Therefore, it is believed that when cells grow in vitro it is better to stretch them both mechanically and electrically. Ideally our device will be able to provide electrical and mechanical stimulation to muscle cells.

There are many objectives that we must meet while stretching the cells. When the cells are being mechanically stretched the cells should reach at a 10% strain. As discussed in the background section, studies have shown that cells have the strongest outcome when they are stretched incrementally over time instead of going straight from 0% strain to 10% strain, for example. Our device should be able to incrementally stretch the cells over time. The cells also need to be stretched about once every second, 1

Hz. It takes the cells about one week to mature while they are being stretched. Our device needs to be able to stretch the cells inside of the wells for the entire one week period.

We are designing a high throughput device to stimulate the cells. Ideally our device would be able to stimulate 96 wells at the same time. By stretching at 96 wells at a time we can run experiments to see if our design actually helps improve the strength of the cells that are stretched. We need to be able to determine the property of the cells over time. We do not need to know the mechanical property of the cells in real time as long as the process can be stopped to determine the strength of the cells throughout the process. In order to do this the device needs to be able to be stopped and held at a desired strain so that the user can take images of the posts to measure the deformation of the tissues.

Lastly, our device needs to be repeatable and reproducible after our project is over with. Our device needs to accurate within 5% of the desired strain by the user. The user has to know that the strain that they are inputting is the strain that they are receiving on their engineered tissues. Our device needs to be used in lab constantly to stretch muscle cells. The goal is to have this device will work for years to come to be used for many different experiments and projects within the lab. This product should also be able to be reproduced in the case that other labs want to use our device to stretch their own cells.

### *3.2.2 Design Constraints*

After reviewing the initial client statement, researching the limitations and successes of similar projects and interviewing the client we came up with the following constraints for our own design. The list of constraints are below in Table 4.

**Table 4: List of Design Constraints**

| **Design Constraints** | **Specification of Constraint** |
|---|---|
| Budget | $1000 |
| Timeline | 28 weeks |
| Operative under conditions in an incubator | 37°C<br>5-7% $CO_2$<br>95% Humidity |
| Fits in an incubator | Size of incubator |
| Sterile | Cannot introduce bacteria when stretching the cells |
| Non-cytotoxic | Cannot damage cells |

| | |
|---|---|
| Stimulation | At least mechanical stimulation |
| Incremental strain over time | Stretch cells at a three strains (2%, 5% and 10%) |
| High throughput | Eight wells simultaneously |

This project must be completed on time and within the budget given to us by Worcester Polytechnic Institute. We have 28 weeks to complete this project and a budget of $1000, $250 per team member. The budget of $1000 is something that is set by Worcester Polytechnic Institute, yet a larger budget can be acquired if the team proposes to the the client how an increase in the budget will greatly improve the overall function of the device.

In order to properly stretch the muscle cells we have to stretch them while they are growing. In order to do this we must stretch them within an incubator that mimics physiological conditions. Therefore, the device must be able to work under conditions of 37°C, 5-7% $CO_2$, and 95% humidity. Since the device must operate within the incubator it will also have to be small enough to fit within the size of the incubator.

Our design and materials that we use cannot damage the cells in anyway while the cells are being stretched. Our design must be sterile. Through stretching the cells, our device cannot introduce any bacteria into the wells. All of the materials that we use need to be non-toxic to the cells. We do not want to kill the cells or damage any of the mechanical properties of the cells by using our device to stretch them.

Although our device should be able to stimulate 96 wells at a time it needs to at least stimulate 8 wells simultaneously at a time. Stimulating 8 wells at a time will allow us to do experiments testing how the stimulation affects the properties of the cells. Once this process if refined then it can better be used on a 96 well plate. This stimulation at least needs to include mechanical stimulation. Ideally this device would be able to both mechanically and electrically stimulate a cell, to closer mimic cells within the body, but having the cells mechanically stimulated would allow for the cells to mature faster in vitro. Ideally these cells would be able to be stretched over a large value of strains, but the cells need to be at least be stretched over three levels, 2%, 5% and 10%.

# Chapter 4: Design Process

## 4.1 Needs Analysis

A needs analysis is used to better understand and identify the most important design objectives according to the client. Often times, the needs of the client and the objective of the device can conflict with one another. Therefore, it is necessary for a need analysis to be conducted to compare and contrast the objectives in relation to one another. The following need analysis, seen in Table 5, was conducted using a pairwise chart to identify the most essential and significant design objectives.

**Table 5: Pairwise Analysis Chart**

| Design Objective | Repeated mechanical strain | Ease of use | Accuracy | Low cost | Greater than 3 strains | High throughput | Total |
|---|---|---|---|---|---|---|---|
| **Repeated mechanical strain** | X | 1 | 1 | 1 | 1 | 1 | 5 |
| **Ease of use** | 0 | X | 0 | 1 | 1 | 1 | 3 |
| **Accuracy** | 0 | 1 | X | 1 | 1 | 1 | 4 |
| **Low cost** | 0 | 0 | 0 | X | 0 | 0 | 0 |
| **Greater than 3 strains** | 0 | 0 | 0 | 1 | X | 0 | 1 |
| **High throughput above 8** | 0 | 0 | 0 | 1 | 1 | X | 2 |

Table 5 above shows the most important design concepts and objectives of our design. Each design objective is weighed against the remaining objectives and given a score of one or zero. A score of one denotes that the horizontal objective is more critical to the clients than the vertical objective in the row. While a score of zero indicates that the vertical objective is more critical to the clients. As demonstrated in the table above, the team has identified that repeated mechanical stimulation with accurate strains to be the important objectives when determining the functionality and operation of our device design. In contrast, the cost of the device was established as the least critical objective. It is important to note, that the displayed need analysis above does not disregard any objective of the design or client desire. Instead, the need analysis chart organizes the influence and significance of each objective on our final design.

Another component of the team's need analysis is a Pugh analysis table. The purpose of this chart is to compare potential design concepts with weighted design objectives. The weights for the design objectives are determined by the significance of the respective objectives based on the pairwise chart as shown below in Table 6. The results of the Pugh analysis will determine the best design concepts based on the device and client objectives.

**Table 6: Pugh Analysis Chart**

| Design Objective | Weight | Magnetic Actuation | Direct Mechanical Actuation | Actuation from Underneath | Dual Linear Actuation | Sliding Posts |
|---|---|---|---|---|---|---|
| **Repeated mechanical strain** | 5 | 0 | 1 | 1 | 1 | 1 |
| **Ease of use** | 3 | 0 | 0 | -1 | -1 | -1 |
| **Accuracy** | 4 | -1 | 1 | 0 | -1 | 1 |
| **Low cost** | 0 | 0 | 1 | -1 | 0 | -1 |
| **Greater than 3 strains** | 1 | -1 | 1 | 1 | -1 | 1 |
| **High throughput above 8** | 2 | -1 | 1 | 1 | 1 | 1 |
| **Total** | | -7 | 12 | 5 | -1 | 9 |

Based on the Pugh analysis chart, the team identified that the most appropriate and advantageous design concept is the direct mechanical actuation. This design concept satisfies the most device objectives as determined by the client. Not only does the direct actuation meet the most design objectives, but it also fulfills the two highest weighted and most critical design objectives. The second highest ranked design is the sliding post design. The chart above shows that it fulfills most of the design objectives, but not all of them. The lowest ranked design was the magnetic post design. This design showed poor accuracy and an inability to produce more than 3 strains, which were both highly valued designed objectives. Therefore, this design meet the least requirements out of all the potential design and has been determined as the least reasonable and compelling design concept.

## 4.2 Industry Standards

There are many different industry standards for medical devices that deal with viable human cells. A common set of industry standards is the International Organization for Standardization (ISO). Below, Table 7 lists some of the industry standards that apply to the device that we made.

**Table 7: List of Industry Standards**

| ISO Standard | Description |
|---|---|
| ISO 22442-2:2015 | Medical devices that use animal tissues |
| ISO 13022:2012 | Medical devices that use viable human cells |
| ISO 13485:2016 | Medical devices |
| ISO 10993:2018 | Biological evaluation of medical devices |
| ISO 7712:1983 | Laboratory glassware - disposable pipettes |
| ISO 9001 | Quality management |
| ISO 20457 | Plastic moulded parts |
| ISO 3664 | Viewing conditions of photography |
| ISO/TR 18931:2001 | Humidity conditions for imaging |

ISO 22442-2 and 13022 cover how viable animal and/or human cells should be sourced, collected and handled. These standards also discuss how these cells should be handled when using a medical device to work with the cells. It also sets up the risk management when dealing with human and/or animal cells. ISO 13485 sets up standards on how medical devices should be designed, produced, installed and serviced. This standard also highlights the importance of risk management when it comes medical devices. ISO 10993-1 sets up standards to assess the biological safety of medical devices and sets standards for what the biological safety of medical devices should be. ISO 7712 discusses how to deal with disposable pipettes that are used to transfer biological materials. ISO 9001 gives a number of quality management principles that laboratories should follow in order to produce a quality product. These principles can be included into designing this system in order to ensure that mechanical actuator is a quality product. ISO 20457 sets what tolerances should be for moulded parts including roughness and flow lines. This can be used for any moulded plastics parts that need to be printed for the actuator. ISO 3664 will be used when we are taking pictures of the cells while they are actuating. This ISO standard discusses viewing photographs on a monitor and looking at the comparison between the transparencies in the picture. ISO/TR 18931:2001 sets tolerances as to what temperature and humidity conditions should be when taking pictures. This is important because for this design the cells will be actuated in an incubator which has a temperature of 37°C and 95% humidity. This can easily affect a camera while it is taking pictures of the cells.

## 4.3 Initial Design Concept

Through brainstorming sessions and discussions between the team and client, the team generated a total of four potential design concepts. The designs were chosen based on a variety of criteria, including feasibility, potential to meet design and device objectives as well as opportunity to explore and investigate diverse methods of tissue stimulation and actuation. The five design concepts the team came up with were, magnetic actuation, pressure actuation, dual linear actuation, direct actuation and sliding posts.

### *4.3.1 Design Alternatives*

Magnetic Actuated Post

The first design concept incorporates magnetic stimulation to actuate a moveable post. Each well will include a fixed and moveable post. The moveable post will have a small nickel magnet injected into the top of the post. A magnetic force will be created by an external magnet outside the well plate that will cause a resultant strain in the tissue model. The strain is applied when the magnet outside of the system attracts the magnet in the moveable post. This pins the post against the grey insert shown in Figure 9 below. In order to achieve at least three strains, different inserts must be made and inserted into the system. The main limitation of this design is that many inserts would be required to vary strain, this complicates the use of the design and rejects the clients design objectives. In addition, the fact that the magnetic post will be pinned against the insert could risk sterility of the tissue models. The advantage of this design is that the current post design would require no adaptations to work in conjunction with the mechanism of actuation.

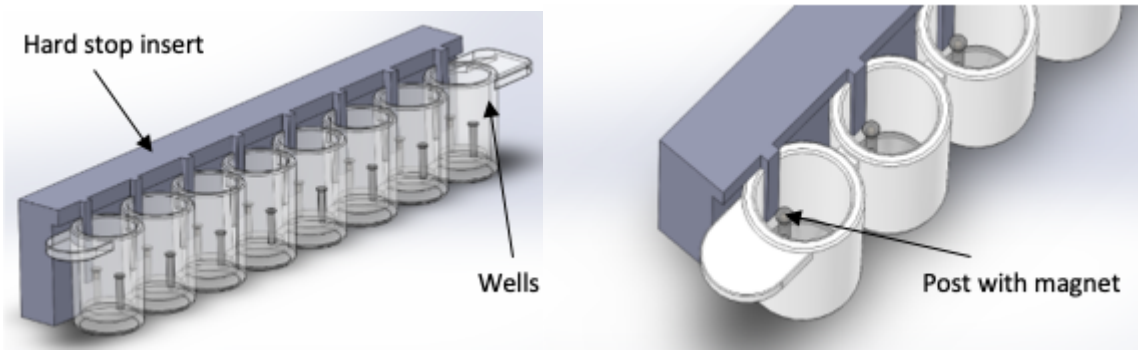


**Figure 9: Magnetic Actuated Post Design**

Magnetic Actuated Post Design. A magnet inserted into the top of the each post will pin the post against the grey magnet hard stop. The hard stop will have multiple sizes to increase or decrease the deformation distance of the post.

Pressure Controlled Actuation

The second design concept the team came up with was a pressurized actuation. This design utilized a flexible membrane on which the posts would be attached to. As the silicon membrane was pressurized using a pump, the membrane would expand, in turn deflecting the posts outwards. This deflection would cause the posts to pull the tissue scaffolds which would cause a strain. Since, air flows from high pressure to low pressure, the team would be able to assume uniform distribution of pressure throughout the well plate. The advantage of this design is that there are no outside or external materials coming in contact with the tissue models directly or indirectly, which eliminates the risk of an unsterile and in-biocompatible environment. This being said, there are many more serious disadvantages associated with this design, such as, axial stretching of the scaffolds, maintaining a vacuum seal between the well plate and the silicone membrane during actuation and lastly a new post and membrane mold. This design can be seen in Figure 10 below.

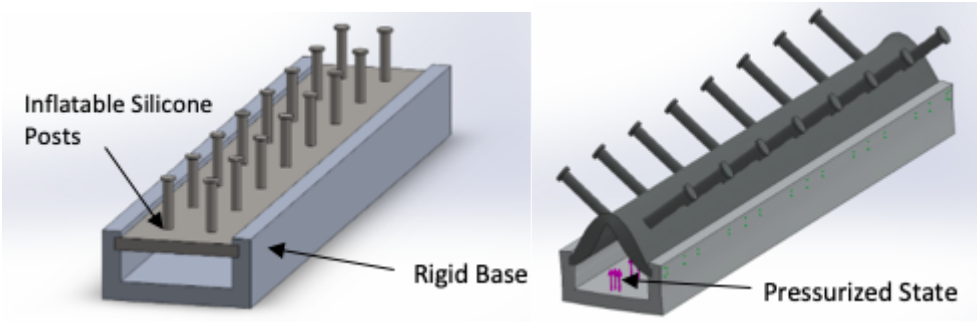


**Figure 10: Pressurized Actuation Design**

Pressurized Actuation. The left image is the unpressurized system at rest, the image on the right depicts the pressurized system and resulting post deflection.

Dual Linear Actuator

The third design is a depressurized system that will linearly pull both sides of a flexible silicone membrane. A vacuum will be attached to the left and right side cavities on either side of the posts. As the vacuum is triggered, the part of the silicone will stretch linearly, which will apply a strain to tissue constructs. The bottom plate will be reusable and be manufactured from a type of metal, while the top plate is made up of PDMS. The major limitation of this design is maintaining a vacuum between the silicone plate and the wells. As the silicone stretches, the vacuum will break and the media in the wells will leak, this will introduce leakage and system contamination. The advantage of this design is that there is no external components that come in contact with the tissue models that could damage the sterility of the constructs. This design can be seen in Figure 11 below.

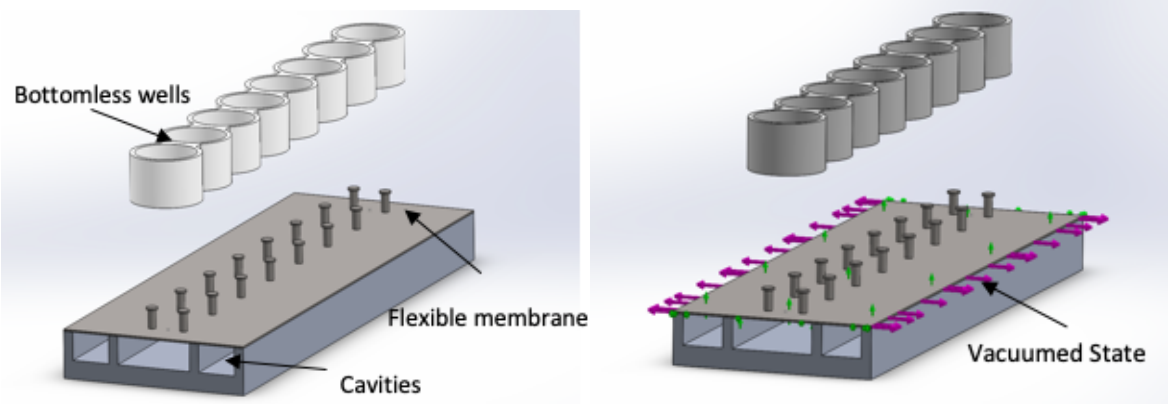


**Figure 11: Dual Linear Actuator**

Dual Linear Actuator. The left image is an assembly of the system at rest. The right image shows the mode of actuation and the subsequent post movement.

Direct Mechanical Actuator

The fourth design concept is the most basic design idea, it utilizes a motor controlled top plate with pins pointing downwards towards the posts. The top plate would be controlled through a software similar to LabView that would be able to program cyclic movements. The pins would be attached to the top plate and be sharp enough to penetrate the center of the posts. Once the posts are punctured, the motor driven top plate would move side to side. As the punctured post moves against the fixed post a resulting strain will be applied on the tissue models. This mechanism of movement is demonstrated in Figure 12 below. The advantages of this design include the use of the existing wells and posts as wells as the ability for the design to incorporate accurate varying strains using the motor. The most challenging aspect of this design is the ability to precisely image the tissues models. As described above, this design requires a bar for the pins to attach to, therefore there is a concern that the bar will affect the quality of the image from above.

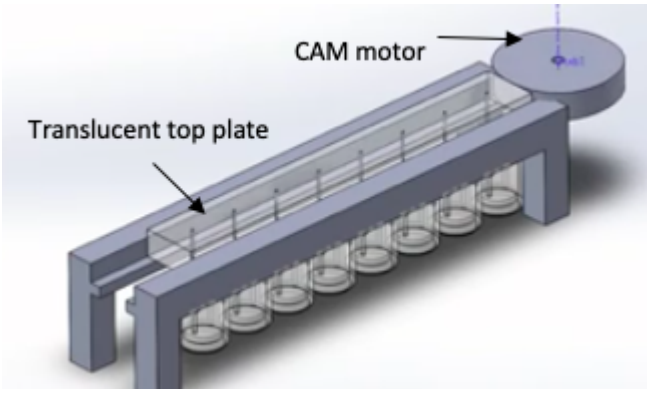


**Figure 12: Direct Mechanical Actuator**

Direct Mechanical Actuator. Pins inserted into one of the silicone posts will be actuated using the CAM motor seen in the right image.

Sliding Post Actuation

The fifth and final design concept incorporates well like plates that slide against each to linearly actuate the posts. The bottom plate will be made of of a plastic or metal that will be flat with one post. The top plate will be made of a silicone with the opposite corresponding post and a circular hole for the bottom post. Finally, the bottom plate will be inserted through the hole in the top plate, such that both posts are at equal heights. A motor will control the movement of the bottom plate, which will slide side to side against the silicon plate. As the bottom plate moves, the tissue scaffold will pull against the posts inducing a strain. Similar to the direct actuation design, the use of a motor allows for much more control and accuracy of the applied strain in this design. On the other hand, this design presents new problems such as, the risk of contamination and leaking of solution through the holes in the silicone plate. This design can be seen in Figure 13 below.

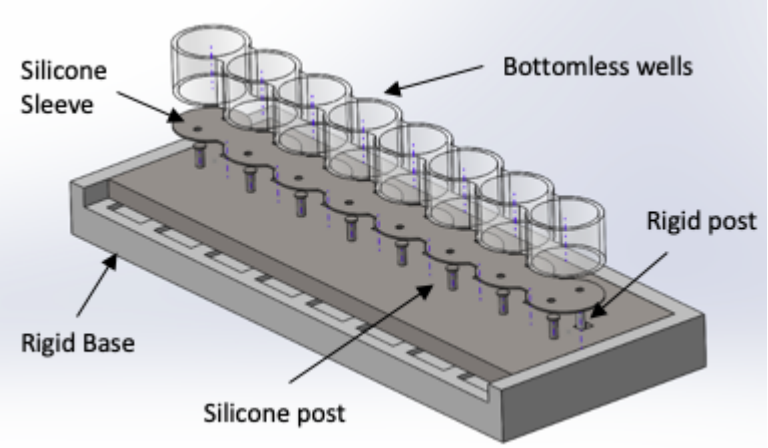


**Figure 13: Sliding Post Actuator**

Sliding Post Actuator. This image shows the assembly of the sliding post actuator, including the bottom plate, top plate, silicone sheet and bottomless wells.

### *4.3.2 Feasibility Testing for Design Alternatives*

The section describes the testing methods the team used to determine the feasibility and practicality of each of the five design concepts as explained above. After reviewing the advantages and limitations of each design with the client and comparing each design with the need analysis the team moved forward with two different designs, the Direct Mechanical Actuator and the Sliding Post Actuation. Each design idea has various advantages and disadvantages that are unique to the design and method of actuation. Therefore, it is essential to conduct early testing to identify which designs will most closely follow the design objectives and constraints that are set in section three above.

For the first design, the Direct Drag Mechanical Actuator, our major concern was being able to pierce the silicon posts with a needle in order to mechanically actuate the posts. In order to determine that this design was feasible we took sewing needles and used them to attempt to manually actuate the posts. Piercing the silicon posts proved to be harder than we originally expected. With enough force though the needles went in straight and did not poke out of the side of the post. This was important to make sure that the needles would not be sticking out, so that they don't puncture the muscle tissue. From this our next feasibility study was to determine if we could form the posts with a needle in them. This would create a small crater in the top of the post which would make it easier for the needle to pierce the post and actuate it.

For our second design, the Sliding Post Actuation, our major concern was that the media would leak out of the bottom of the siding post. Our original idea was to have a trough to catch the excess media. This is not idea because it would cause the user to constantly have to add more media to the well, which could be a waste of time and money. Our next idea was to put a sleeve over the post that would move with the post. In order to test this out we 3D printed part of this design out at a larger scale, this is shown in Figure 14.

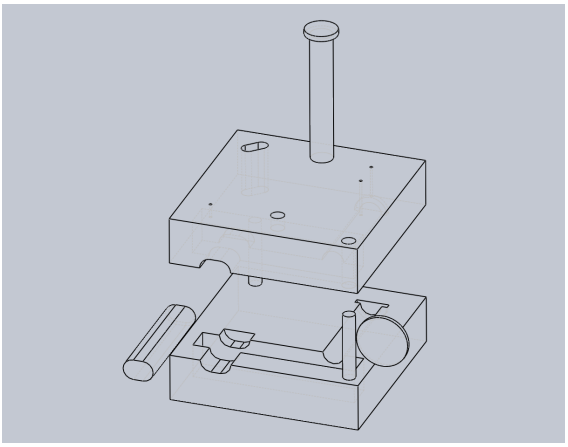

**Figure 14: Solidworks Drawing of Sliding Post Test Mold**

Although this helped to minimize the amount that was leaking some liquid could get through. The team decided, this could become problematic when put on a larger scale, such as when doing 96 wells at a time versus the one set of posts that we did a test on.

Based on the feasibility tests performed and the Pugh analysis chart found in table 7, the team decided that the direct mechanical actuator design satisfied the most design objectives and made the most sense moving forward.

### *4.3.3 Design One*

The second design phase took the best design from phase one based on design objectives and client comments. The direct actuation design was elaborated on to incorporate two stepper motors, one linear actuator, one cam motor, and fifteen pins. The device had an imaging window that would allow for a picture to be taken, while the bottom plate moves from well to well. The linear actuator moves the top assembly up and down as the pins move in and out of the wells. The smaller linear actuator is attached to a cam motor that moves a sliding plate back and forth against a spring, actuating the pinned posts. The Solidworks model of this design is shown below in Figure 15.

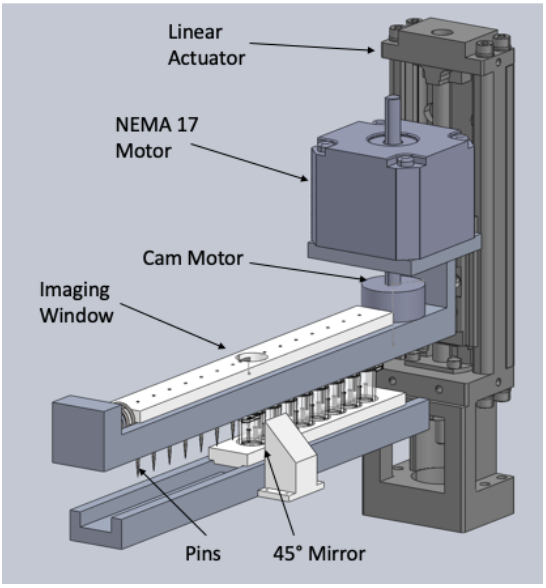


**Figure 15: First Design of the Direct Mechanical Actuator**

In the end the team did not move forward with the design due to it's foreseen limitations. The most concerning limitation associated with the direct mechanical actuator was contamination of the scaffolds and media due to the frequency of removing and re-piercing the pins. The media and the scaffolds are both very sensitive and it is imperative that both stay contained and sanitary throughout the incubation and media changing process. In addition, it seemed unrealistic for the needles to continuously re-pierce the posts without damaging the scaffolds. The main advantage of the design was that it utilized the current posts and well mold.

### *4.3.4 Design Two*

In the second design phase, the team attempted to address all of the limitations and concerns of the first design while also focusing on meeting the design objectives and requirements. The second design uses eight inch and a half ninety degree bent needles. The team chose bent needles to allow for images to

be taken from above. Similarly to the first design, the second design also uses a stepper and cam motor to actuate the needles. To address the concern of needle and media contamination from the first design, the linear actuator instead move the entire actuating assembly side to side for well imaging. This design can be seen in Figure 16 below.

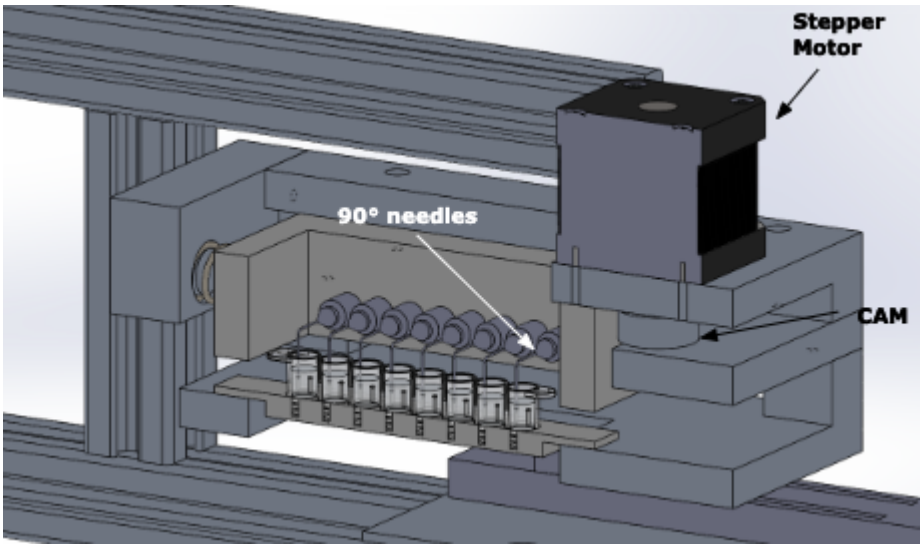


**Figure 16: Second Design of the Direct Mechanical Actuator**

After careful thought and consider, the team and clients concluded that the second design did not meet some of the design objectives. The three main issues with the design was that it was too big and bulky for the clients ease of use, the open top could cause contamination of the media and the bent needles were not stiffness enough to actuate the posts. For the clients purposes and research environment, the device must be able to fit into a 20x20 incubator. Therefore, this design failed to meet the needs of the client. In addition, the open top designed for imaging purposes was discovered to cause contamination of the media and scaffolds. Lastly, the team found that the stiffness of the bent needles did not exceed the stiffness of the posts by very much. In attempt to fix this design flaw, the team decided to use straight needles to puncture the posts from above. The mechanism pictured below was designed in attempt to puncture 8 posts simultaneously.

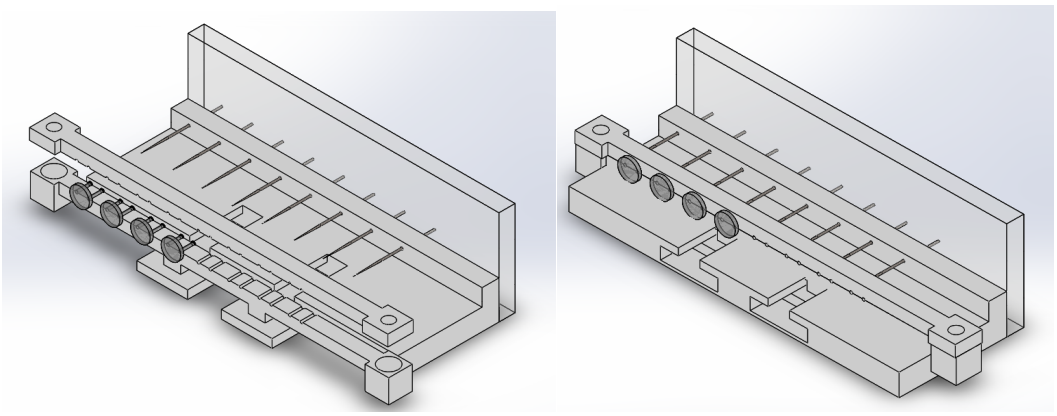

**Figure 17: Fixture to Pierce Posts with Needles. Two piece mold clamps down on posts shown in darker grey. Mold slides along rail until all eight posts are punctured.**

The 3D printers our team had access to unfortunately did not have precise tolerances needed to hold the posts rigid enough for the needles to successfully puncture them. We also found that with every failed attempt to puncture the posts, the more dull the needles became, making the process even more difficult. Due to the dullness of the needles and struggles of the mechanism, the few needles that did puncture the posts were not deep enough in the PDMS to remain in that position. After being placed in the actuating unit, the needles slipped out from the posts due to the dynamic nature of the system and forces acting upon them. Based on these three main issues and challenges, the team and client decided not to move forward with this design and started on the third design phase process by taking the advantages that the second design provided and building upon it.

# Chapter 5: Final Design

## 5.1 Design Overview

For our final design we chose a modified version of the Direct Mechanical Actuator. After reviewing the strengths and limitations of our final two designs and comparing each design to our design objectives and constraints, the Direct Mechanical Actuator most closely satisfied our project needs. The final product was designed with intent of being compact and suitable to the users environment. The final design incorporates a two part model, which includes an actuating unit and an imaging unit. The actuating unit is responsible for cyclically stimulating the tissue constructs and maintaining a sterile and compatible environment. The imaging unit is responsible for providing the user with an imaging mode, such that they can take pictures of the scaffolds during actuation to be analyzed for stress and strain values. All moveable components are controlled using an Arduino Mega, which the the user uses to choose between a cyclic or imaging mode. The Arduino code can be found in Appendix A.

### *5.1.1 Actuating Unit*

The actuating unit consists of a well base, a clear polycarbonate needle holder, and a cam motor that is controlled by a NEMA 17 stepper motor. Eight bent needles, which are 0.6mm in diameter and 26mm long, are attached to the rectangular clear acrylic plate.  Our team bent the bottom of the needles in order to accommodate for the issues experienced while trying to puncture the posts described in section 4.3.4.

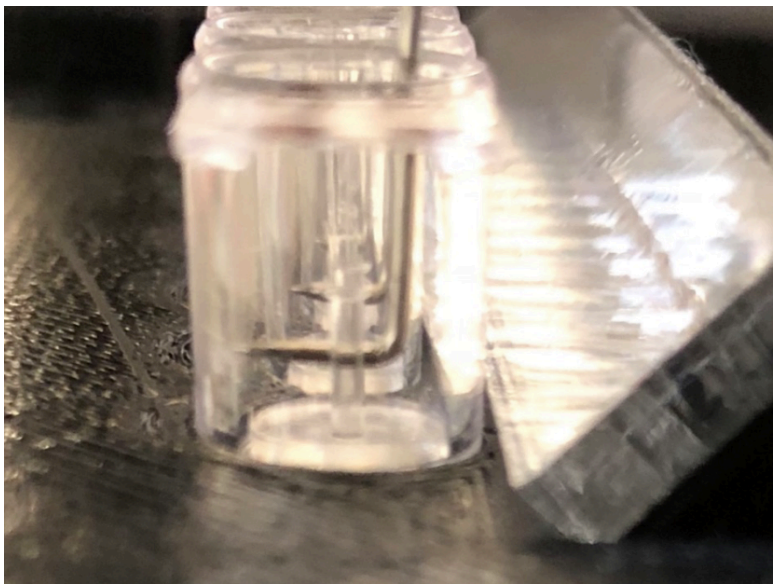

**Figure 18: Bent Needles for Final Design**

The following calculations were performed to assure that the stiffness of the needles were adequate compared to the stiffness of the posts in order to cause accurate strain and deflection. The calculations are shown below, equation one shows the stiffness of the posts, while equations two shows the stiffness of the needles. The needles were found to be 209 times greater stiffness than required.

$$k_{post} = \frac{3EI}{L^3} = \frac{3E\frac{\pi r^4}{4}}{L^3} = \frac{3*(1.0\times10^6)*(\frac{\pi*0.00040^4}{4})}{0.0039^3} = 1.0N/m \quad (1)$$

$$k_{needle} = \frac{3EI}{L^3} = \frac{3E\frac{\pi r^4}{4}}{L^3} = \frac{3*(193\times10^9)*(\frac{\pi*0.00030^4}{4})}{0.026^3} = 210N/m \quad (2)$$

During actuation, the cam motor pushes the needle plate back and forth against a spring causing a deflection on the posts. The user initiates this by using a keypad and LCD to choose between a cyclic mode or a imaging mode. The cyclic mode allows the user to then input their desired frequency, strain and duration of the desired test. There are some set in maximum values for the frequency, strain and duration. The maximums are set to ensure that the user isn't accidentally damaging the tissue by stretching it too much, too fast or too long. The maximum values were set at 15% for the strain, 3 Hz for the frequency and 24 hours for the duration of the test. Next, an eight strip well plate is snap fitted towards the bottom of the assembly beneath the needle tips to the well base. To ensure sterility and biocompatibility the well plate environment is completely enclosed to ensure that no bacteria could flow in and contaminate the scaffolds. In addition, the clear acrylic plate that holds the needles also has slotted holes on the top to allow the user to insert pipettes and aspirators through to the wells to change media. Finally, a strip of 45 degree mirrors are placed alongside of the bottom housing to allow for top and side images to be taken at once. A solidworks model of the actuating assembly can be seen below in Figure 19.

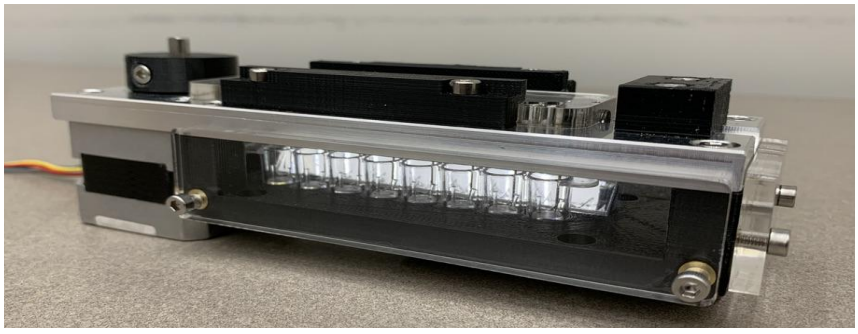

**Figure 19: Actuating Unit**

Actuating Unit. This figure shows the current design of the assembly. The design incorporates a stepper motor-driven cam. The cam controls the linear motion of an acrylic bracket to which the needles are mounted. The needles are inserted into each well, applying strain to the tissue as the cam rotates. The

design allows for imaging from above through the acrylic plate as well as through the open front and back side.

### *5.1.2 Imaging Unit*

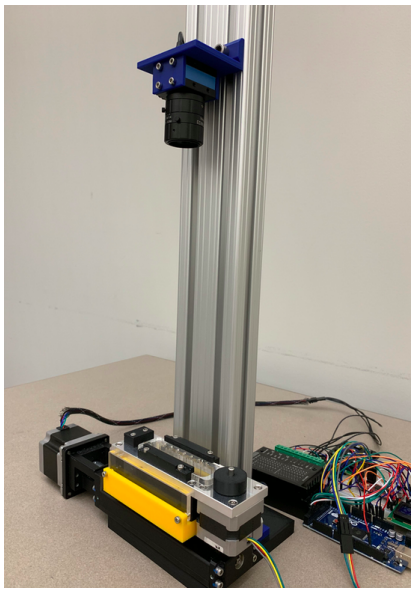

**Figure 20: Imaging Unit**

Imaging Unit with Actuating Unit attached. The height of the camera and lens are adjustable so that the working distance can be adjusted during imaging. The linear actuator rest on the base of the stand and moves the actuating unit side to side to image all eight wells.

The imaging unit is comprised of a THK KR26 linear actuator with a 70mm travel distance that is controlled by a NEMA 23 stepper motor attached to an adjustable camera mount. The imaging unit also includes a high resolution machine imaging camera and len. The adjustable camera mount allows the user to change the working distance of the lens depending on the type of lens being used and the image being taken. The imaging mode is initiated when the user selects imaging on the keypad and LCD screen. This mode allows the user to control when the scaffolds is in its stretched state and pauses the program allowing the user to take a picture. After the user takes a picture and returns the scaffold to its relaxed position, they can select to move to the next well using the keypad. Once this is selected, the NEMA 23 stepper motor rotates the linear actuator to the position of the next well. This process will continue until the user is satisfied and all pictures of the wells have been taken.

The images are taken using *DMK 37BUX178 USB 3.1 monochrome industrial camera* from the Imaging Source. The camera is attached to a *55mm FL Partially-Telecentric Imaging Lens*. During imaging, LED lights will illuminate the bottom of the wells allowing for a clear image and contrasting image. The camera was chosen by the team and client based on its resolution and frame rate. The client specified that the camera must be greater than 1000 x 2000 pixels based on the clients need to measure

ten to twenty five microns of displacement. This was determined by assuming that the picture taken must be 10mm x 20mm given that the diameter of the well is 7mm. From here, the relationship between the length of the field of view and microns displaced was determined using the following equation.

$$10mm \div 10 \frac{microns}{pixel} = 1000\ pixels$$

Therefore, based on the clients prior imaging experience, the team and client decided that the resolution must be at 6 megapixels or above. In addition, the camera must be able to take pictures at a stretching frequency of 1 Hz. In addition, the camera must have a minimum frame rate of thirty frames per second. Given these requirements and specifications, the team and clients with much thought and consideration purchased *DMK 37BUX178 USB 3.1 monochrome industrial camera* by the imaging source.

The camera lens was also extremely important to the final device design and making sure that the device operates correctly and to the clients standards. The two main requirements of the imaging unit were that it must be perform its function as compact as possible, meaning that it must fit within the incubator. Therefore, the lens must have a short working distance, with a wide field of view and high depth of focus. In addition, the wide field of view must not increase the distortion of the lens by a significant amount. Based on these specifications and needs, the team decided to purchase the *55mm FL Partially-Telecentric Imaging Lens* from Edmund Optics.

## 5.2 Well Plates

For this design we are not changing the well plate design that is currently being used in the client's lab. Currently this includes an eight well strip. Each well is 8.62 mm in diameter and 10.7 mm deep. Each well is connected to another to make a strip of eight wells. The well strip is made out of a clear plastic. A CAD design of the well strips can be seen below in Figure 21.

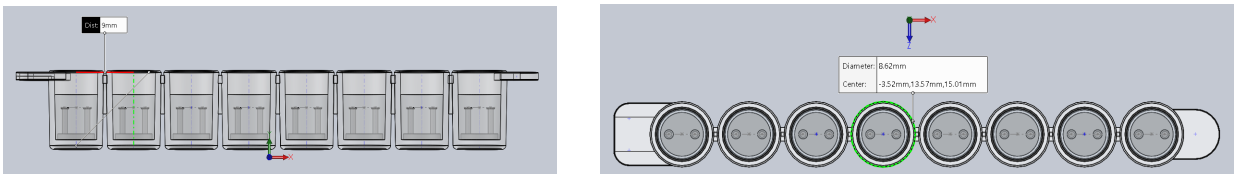


**Figure 21: Solidworks Drawing of an Eight Well Strip**

At the bottom of the wells is where the posts are glued in using uncured PDMS. The media and scaffolds are then grown on top of the posts inside of each well.

## 5.3 Posts

For this design the posts are the same as the posts that are currently used in the client's lab. These posts are made out of PDMS. There are two posts connected at a base. The base of the post design ensures that each of the posts are equal distances apart from one well to the next so that when one of the posts is actuated then each well will be receiving the same strain for a set distance that one post is moved. Each post is located 3.5 mm apart, from the center of post to the center of the next post. Each post is 3.9 mm tall with a diameter of 0.8 mm. At the top of each post is a cap that is 0.2 mm tall with a diameter of 1.2 mm. This cap is to help prevent the muscle tissue from slipping off of the posts because the tissues tend to move up on the posts so if there is nothing there to cap it off then it will slip off. The post design can be seen below in Figure 22.

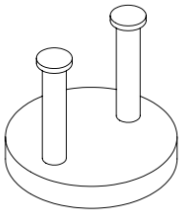

**Figure 22: Solidworks Drawing of the Post Design**

One aspect of the current post and well design that the team optimized was the process of which the posts are attached to the well plate. One important feature of the team's design is the fact that each set of posts in the well strip must be centered and straight in the well. Therefore, the team designed a fixture to load the posts in the well. The fixture pinches the top of the posts which are held in place using two screws on either side. The fixture is then inserted into an eight well strips with drops of PDMS at the bottom. After a few minutes, the screws securing the fixture are undone and one side of the fixture is removed from the well. The second side of the fixture stays inside the wells for another few minutes, letting the PDMS settle just a little more. Finally, the second side of the fixture is carefully removed and the wells are placed inside an oven at 60°C for two hours to let the PDMS cure. The process can be seen in Figure 23.

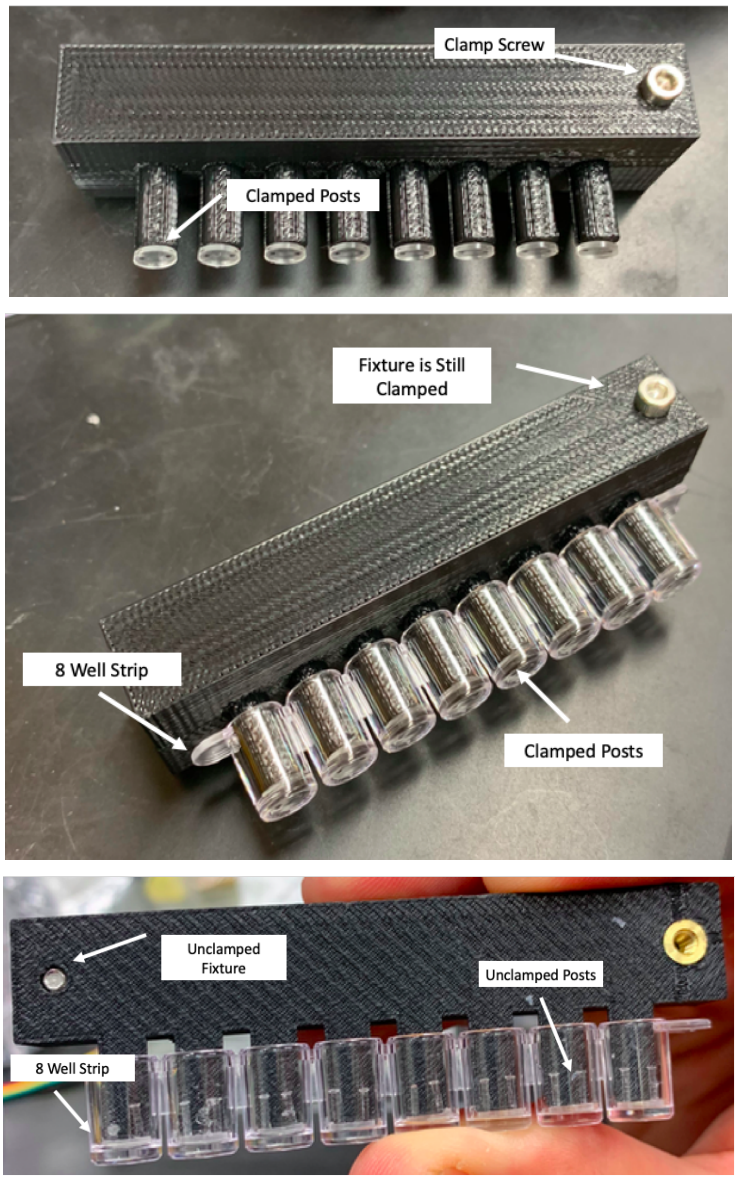


**Figure 23: Post Alignment Fixture**

Post Alignment. Top Picture- The posts are clamped between the two halves of the fixture. Middle Picture- The fixture with the posts clamped in are then placed into the wells with PDMS on the bottom of the posts. Bottom Picture- The fixture is removed from the posts one side at a time.

## 5.4 Tissue Final Design

The muscle tissues that will be actuated with this device will be grown using the same process that is currently being used in the client's lab. A flowchart of how the tissue is casted can be seen in Figure 2 in the background section above. Once the muscle tissue is casted then the tissue can be mechanically actuated. The tissues need to grow for a minimum of 24 hours in the media before they can be actuated. Once the tissue has formed completely around the post it will be mechanically actuated

within the fresh medium as the cells continue to mature around the post. The process of growing the tissues is the same as what was previously done in the Billiar lab, it is now just the addition of being casted in our device. This process will then follow the ISO standards 22442-2 and 13022.

One important consideration the team addressed regarding the functionality of the final design was the process of growing the scaffolds and changing media throughout the duration of scaffold testing. The team overcame this challenge by adding slots in the top of the polycarbonate that holds the needles. The slots allow the user to insert micropipettes as well as aspiration pipettes through the polycarbonate top to change the media every day in the individual wells.

## 5.5 Design Sterilization

One important consideration for this design is ensuring that we are maintaining a sterile environment. If bacteria get into the wells it can affect the muscle tissue and can cause the tissues to die. Therefore, the materials of this device need to be sterilized, especially the top unit. The parts that are most likely to contaminate the wells are any parts that are touching the wells or above the wells. This includes the acrylic top with the needles in it and the aluminum part that hold the motor, acrylic top and the spring. Aluminum and acrylic were chosen for these materials because they can be autoclaved. The rest of the top unit is made out of PLA, which is resistant to ethanol. PLA can be sprayed down with 70% ethanol to get rid of most of the bacteria. The sides of the top unit are covered with acrylic pieces to prevent any bacteria from coming in from the side. Over the entire top unit is an acrylic cover. This ensures that the acrylic piece with the needles remains sterile for when the user has to change the media in the wells everyday.

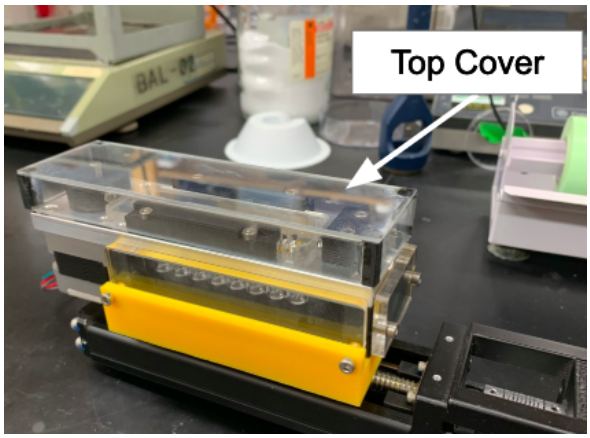


**Figure 24: Actuating Unit with Top Cover**

Actuating Unit with top cover to maintain the sterile environment of the wells and scaffolds while the device is in the incubator.

## 5.6 Design Limitations

The team's final design meets all of the design constraints that are listed above in section 3.2.2, but it does not meet all of the design objectives that were listed in section 3.2.1. In addition, throughout the term the team discovered new and emerging limitations of the device that were not foreseen by the team or clients.

The two design objectives that were listed in Table 4 that the team was not able to meet was objective for mechanical and electrical stimulation and the high throughput objective. For both of these objective the team was only able to meet the minimum constraint which was mechanical actuation and eight wells at a time. That being said, the team believes that final design could be modified slightly for a higher throughput system given more time. The two design limitations that the team did not forsee was in regards to the camera's operating temperature and a compression mode for the actuator. The purpose of this device is to actuate and exercise tissue scaffolds over the course of days and even weeks. Hence, the device must remain inside the incubator at a temperature of 37°C with a 85% humidity for the same amount of time in order to remain sterile. Although the camera has a maximum operation temperature of 45°C, it is still not recommended to store the camera for prolonged amount of times at this temperature. Therefore, the camera must be able to attach and detach from the device to be able to store at a lower temperature. Lastly, the client expressed a desire for the device to compress as well as strain. Since, this was a late discovery by the client, the team and client agreed that this feature not be required in the final design, but might make for a future direction.

# Chapter 6: Device Verification Testing

## 6.1 Test Method

This section outlines how we verified our device to ensure that it met all of our design constraints. We used our test methods to ensure that our device worked accurately within the environment of an incubator so that we could provide accurate data. We also tested to make sure that our device did not harm the muscle tissues that we were actuating.

### *6.1.1 Strain Accuracy Test*

The purpose of this test is to demonstrate that the cells are being stretched to the desired strain. The user inputs a desired strain on a keypad. This value is then coded to correspond to a certain rotation of the stepper motor. This test ensures that the value entered on the keypad is equal to the strain that is performed on the post.

First the user will take a picture of the posts within the wells so that a starting position of the posts can be determined. Then the user will enter a strain of 1% on the keypad. The Arduino will be coded to bring the post out to the 1% strain and hold it there in order for the user to take a picture of the posts. This second picture will again be used to determine the position of the posts. The difference of the positions of the posts can be used to determine what the strain on the post was from the cam and stepper motor. This process will be repeated ten times for ten different strains. We will be testing the accuracy for 1%, 2%, 3%, 4%, 5%, 6%, 7%, 8%, 9% and 10% strain, which will allow us to make sure that our code works for low, medium and high strains. The average and standard deviation of the the tested strains will be compared to the input strain. Adjustments to the code will be made if the average observed strain is greater than ± 5% of the input strain. If the code is adjusted the test will be performed again.

### *6.1.2 Camera Accuracy Test*

The purpose of this test is to ensure that we are getting the most accurate measurements of the posts from the camera. The curvature of the well causes the measurements of the posts to be distorted. This test allows us to determine how distorted the measurements are and if attaching a flat slide with pdms on the side of the well plate helps to correct for this distortion.

In order to test how the curvature of the wells distorts the measurements of the posts we will be using Pocket USAF Optical Test Paper. This test paper is designed to have alternating black and white strips that are exactly 1 mm in width. We will use a small piece of this test paper and place it within the well and the center of the well. We will take a picture of the well from the side and analyze the picture by

using Image J to measure each stripe within the well. Using Image J we will be able to determine how many pixels are within each stripe. If the amount of pixels changes of the stripes from the center of the well to edge of the well we will be able to determine how much the curvature of the well distorts the measurement in the picture. We will then fix a flat slide to the well using PDMS. We will take a picture after the flat slide is fixed and determine if and how much this corrects the distortion that is caused by the curvature of the well.

## 6.2 Results

### *6.2.1 Strain Accuracy Test*

The user inputted strain on the keypad for the arduino was tested at ten different strains between 1 and 10% strain. When the test was first run the accuracy of the strain was off, so the code on the arduino was adjusted to make sure that the measured strain better reflected the strain inputted by the user. The team used a linear relationship between the user input strain and the linear displacement of the needles. The required linear displacement was then converted to a radial rotation on the cam using a sinusoidal equation. Using these equations, the team was able to assemble a larger equation within the arduino code that would relate the user input strain to the accurate cam rotation, which results in the linear displacement of the needles. The linear relationship between the input strain and needle displacement is shown in equation 1. Equation 2 describes the sinusoidal relationship between the linear displacement and the cam. Finally, equation 3 represents the larger equation that converts input strain to cam rotations, additional information on these equations can be found in Appendix A and B. In all of the following equation a denotes user input strain.

$$2.755*a-2.513 \quad (1)$$

$$\text{Angle} = 180°\text{asin}(0.125*(\text{Strain}-8))+90° \quad (2)$$

$$\text{asin}(0.125*(2.755*a-2.513)-1)*57.296+90)*4.444 \quad (3)$$

Equation 3 is used in the arduino code to find the required cam rotations given a specific strain inputted by the user. To validate that the code was accurate we ran the accuracy test ten times to test the strains between 1 and 10%. The average measured strain and standard deviation of the ten strains can be seen in Figure 25 below.

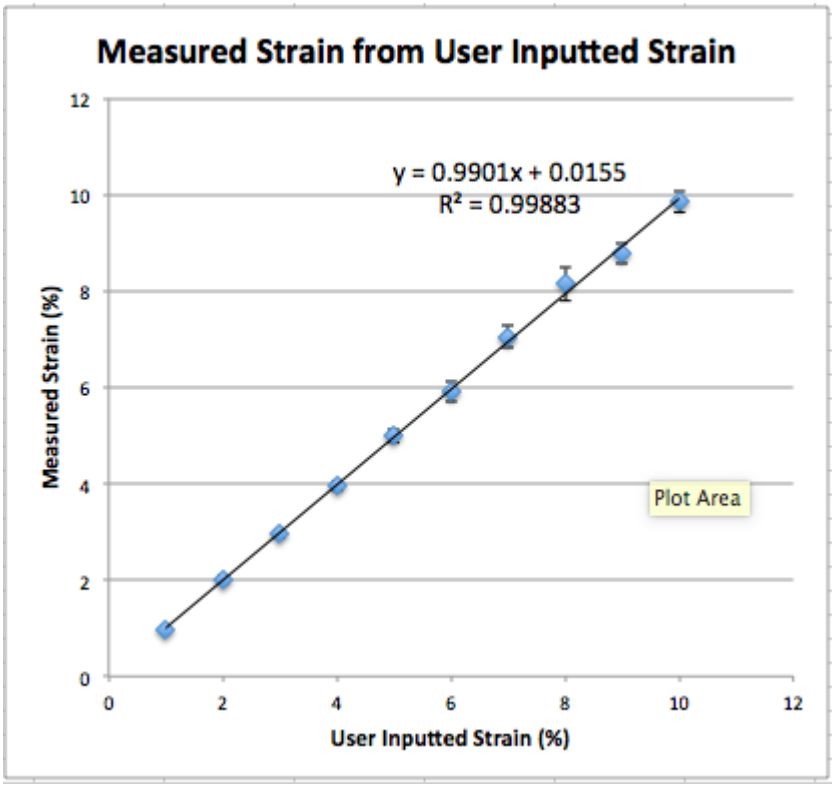


**Figure 25: Measured Strain vs. User Inputted Strain Graph**

It can be seen in the graph above that the slope of the the trendline is 0.99 which is extremely close to 1. All of the data points also fall closely to the trendline, which can be seen with the $R^2$ value of 0.99883. An ANOVA test was run on regression line used for the strain accuracy test. We obtained a P-value of 5.2329E-16, which means that the slope of our line is statistically significant. The data for the ten different strains can be found in Table 8 below.

**Table 8: Strain Accuracy Test Data**

| Inputted Strain | Average Measured Strain | Standard Deviation | P-Value | Percent Accuracy |
|---|---|---|---|---|
| 1% | 0.979% | 0.0402 | 0.0650 | 3.753% |
| 2% | 2.019% | 0.0891 | 0.262 | 3.823% |
| 3% | 2.947% | 0.0760 | 0.0274 | 2.111% |
| 4% | 3.955% | 0.104 | 0.102 | 2.265% |
| 5% | 4.987% | 0.139 | 0.386 | 2.359% |

| | | | | |
|---|---|---|---|---|
| 6% | 5.895% | 0.207 | 0.0709 | 2.969% |
| 7% | 7.053% | 0.228 | 0.241 | 2.260% |
| 8% | 8.154% | 0.355 | 0.102 | 3.494% |
| 9% | 8.769% | 0.214 | 0.00384 | 3.177% |
| 10% | 9.854% | 0.220 | 0.0327 | 2.144% |

All of the percent accuracies of this test were within 5% of the inputted strain, which was the goal for this particular test. When doing a t-test on the different strains it was found that some of the strains were statistically significant and others were not. 3%, 9% and 10% strain were statistically significant, which means that the average measured strain is equal to the user inputted strain. It is recommended that a larger sample is taken so that all strain values are statistically significant. When the stiffness of the tissues is added to the posts the accuracy of the inputted strains will most likely be off and the accuracy test will need to be re-run. The equation for the degree that the cam will need to be turned will need to be edited so that the accuracy of the inputted strain matches that of the measured strain.

### *6.2.2 Camera Accuracy Test*

The device was set-up to image the wells from above, looking down at the tissue constructs forming across the posts. Due to media forming a meniscus with the edges of the wells, there is a magnifying effect when the wells are imaged from above. To amend this, the design features a mirror at a $45^{o}$ angle adjacent to the wells. This allows the wells to be imaged from both the top and the side simultaneously side by side as seen in Figure 26.

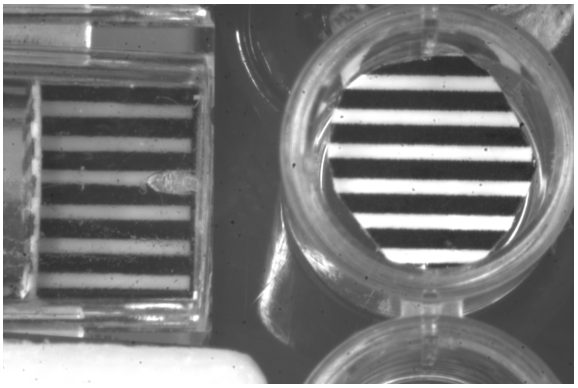

**Figure 26: Image of Top and Side View of Well**

When imaging from the side, the surface-level meniscus no longer impacts the image of the tissue construct. That being said, imaging from the side introduces new challenges to the set-up. From the side,

light is refracted through three media (air, polycarbonate wells, and growth medium) before reaching the tissue. Figure 27 below shows the direction that the light paths as they pass through the well to the post. The index of refraction of air outside of the well is around 1, the index of refraction of the polycarbonate well was 1.60 and the index of refraction of the media is similar to water so it is approximately 1.33. This difference in the index of refractions as the light moves from outside of the well to inside of the well causes there to be an appeared magnification of the posts inside of the wells.

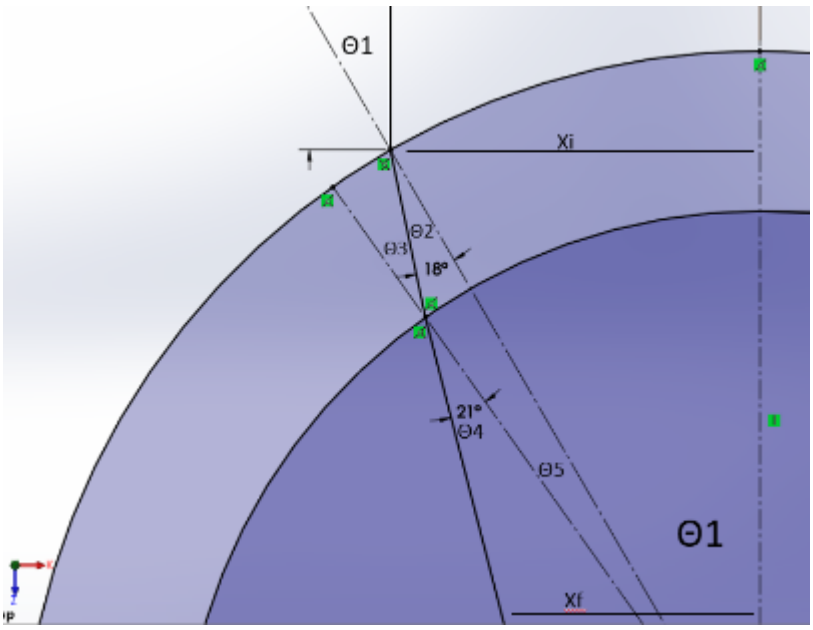


**Figure 27: Light Path for Side of Well**

Light path traveling from outside of the well to the inside of the well. The light has to pass through three different media (air, polycarbonate and growth media), which causes a magnification affect.

To account for this magnification, an equation was developed to calculate the true location of the tissue compared to the magnified location. This equation was derived using the curvature and thickness of the wells in addition to the refraction equations through each medium. Figure 28 shows the resulting plot of true position vs. imaged position as well as the best fit line used to simplify.

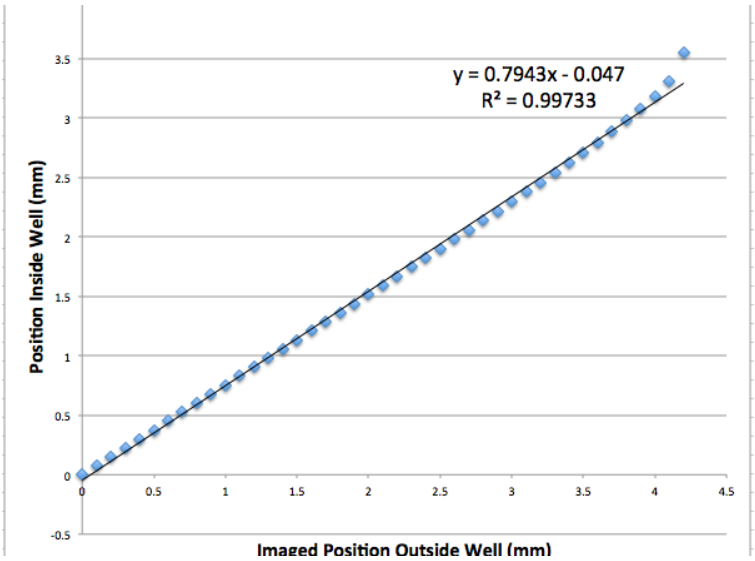


**Figure 28: True Position vs. Imaged Position Graph**

Within the working distance of strains that will be applied to the posts the observed position that is imaged follows a linear fit to the actual position of the post inside of the well. The imaged position closely fits the actual position of the posts inside the wells to an $R^2$ value of 0.99733, which means that all of the points lie very closely to the best fit line that was found. This means that there is a constant magnification of the imaged position and the actual position of 1:0.7943, as can be seen in the graph above. An ANOVA test was run on regression line used for the camera accuracy test. We obtained a P-value of 1.83102E-16, which means that the slope of our line is statistically significant. This constant magnification can be used when analyzing the side view images of the wells to determine the actual distance of the posts within the well.

# Chapter 7: Discussion

The main objective of this Major Qualifying Project was to improve the current process of manual actuation being done in the Billiar Lab at Worcester Polytechnic Institute. In the Billiar Lab currently scaffolds are actuated by a user with a small tool pushing one of the two posts away from the other causing the both posts to deflect. The deflection of the posts are used to calculate strain and force applied to the scaffold. This does not allow the scaffolds in the Billiar Lab to be actuated in a dynamic and cyclic manner. Additionally, this process only allowed for actuation and calculations to be performed on one well at a time. It also was not possible for the results to be consistent, reliable, or repeatable.

Our device meets all of the design constraints set out for us from our client. We created a device that will mechanically actuate eight wells at a time. The user has the ability to enter different strains and frequencies for the device to actuate at. This can allow for the the engineered tissues to be stretched over time by increasing the strain that is applied onto the tissues. This device is compact enough to fit within the incubator, and if using long jumper wires for the arduino parts to stay outside of the environment of the incubator, can operate within the temperature and humidity conditions of the incubator. We also made sure that our device could be sterilized. Any parts that had any chance of coming in contact with the posts or the pipettes when changing the media daily were autoclaved and all other parts are resistant to ethanol and can be wiped down with 70% ethanol.

In order to ensure that our device was repeatable and reproducible we conducted an accuracy test on ten different strains. On the posts alone, not in media or with scaffolding surrounding them, our device proved to be within 5% accuracy of the strain that the user inputted. This test will need to be redone and the equation used for the cam in the Arduino code will most likely need to be changed once the test is run with engineered tissue scaffolds on the posts. Our device was used to stretch an engineered tissue scaffold and did not rip the scaffold or cause it to come off of the post.

# Chapter 8: Project Impact

This sections investigates the impact that the project has on the environment and society as well as the ethical and safety concerns associated with the project. The goal of the section is to address the social responsibility of the team in relation to the cost, material, manufacturing practices and health and safety of the user.

## 8.1 Economics and Manufacturability

The final design of this project was designed with cost and manufacturability in mind. Therefore, the final design used inexpensive material with manufacturing techniques that were simple, repeatable and cost effective. The final design was made using a mix of additive manufacturing and CNC machine, both of which are relatively inexpensive and fast processes. The additive manufacturing parts were made of polylactic acid (PLA) material. This is one of  most common material used in 3D printing due to it being readily available and its inexpensive cost. The 3D printed parts that were made out of PLA followed the ISO 20457, so it follows the set tolerances and flow of the 3D printing machine. The CNC machined parts are made from Aluminum. The team chose Aluminum for the reusable parts for its ability to withstand ethanol baths and UV light sources. Aluminum also proved beneficial for its lightweight and cost effectiveness. Additive manufacturing is ideal for fast and repeatable parts, however, cannot be reused which produces a lot of waste. Therefore, the team decided to CNC as many parts as possible in order to produce a reusable system that would limit waste and additional costs from over manufacturing.

Throughout the design phase, the team prioritized a simple and small design. The simplicity of the design allowed the for fast and inexpensive manufacturing. The small size of the design also meant that the team did not waste a lot of material. It was important to the clients to have a small design in order to for the device to be compact enough to store in small spaces.

The budget for this project was $1000. Our client however felt that it was important to purchase a new lens and a new camera to better image the wells, so we went over budget in order to purchase a higher quality camera and lens that would aid in measuring the deformation of the tissues. Below, in Table 9, shows a cost break down of each section of our device. The actuating unit refers to the unit of our device that hold the wells directly and stretches the posts. The arduino parts cost refers to the Arduino Mega that is holding our code, the keypad, LCD display and the motor drivers. The imaging unit refers to the linear actuator unit that moves the actuating unit from side to side so that each well can be imaged.

**Table 9: Cost Analysis for Device**

| | Price |
|---|---|
| Actuating Unit | 86.56 |
| Arduino and Electronic Components | 150.25 |
| Imaging Unit | 238.74 |
| Camera, Lens and Camera Mount | 1151.88 |
| **Total** | **1627.43** |

A complete list of all of the components and materials that are used along with their individual prices and a link to where the team purchased the component can be found in Appendix G. Without the lens and the camera the cost of our device and camera mount costs $532.43, which is under the budget for our design. The actuating unit works independently of the imaging unit and can be attached or detached at any point throughout the process. Therefore, only one imaging unit is needed but there can be multiple actuating units that will stretch multiple eight well strips. The only change would be the use of the electronic components, with the addition of a motor driver for the linear actuator. The cost of our actuating unit and all of the arduino components that would be needed to actuate the posts would come to $221.91. When manufacturing multiple units at a time, 12 for instance which would bring the throughput up to 96 wells, the cost for the actuating unit can be dropped significantly, down to $59.77. Making multiple units offers a large price reduction because materials that are needed to buy the unit can be bought in bulk, which saves on price. Some of the materials needed for the initial unit provides enough materials to make all 12 units, such as the material bought for the mirror. Additionally in the initial unit a power supply that can be plugged into the wall was used. This component was expensive, but a cheaper 12V battery could also be used to power the system. To get the cost of $59.77 for the actuating unit 12V batteries were used instead of the cost of the power supply. Batteries would need to be replaced every so often, which could be problematic is the Arduino stopped running in the middle of a test, so a power supply was used instead.

## 8.2 Environmental Impact

The environmental impact of the final device is extremely and low and does not increase the waste produced by the current process. The device itself was designed and manufactured with the intent of being reusable. Therefore, the team chose material that could be sterilized for multiple uses. On the other hand, the process of sterilizing the device does cause ethanol waste and requires the use of a UV source. In large quantities UV light is not good for the environment and has been proven to be harmful to

the earth's atmosphere, however for the level of exposure used in our project, the team does not see any long term effects of the process. In addition, UV light is a commonly used lab practice for a variety of uses. Ethanol is disposed of using chemical waste containers often found in labs. From there, proper waste management techniques that are employed by WPI's Gateway lab to safely dispose of the ethanol. Ethanol is not harmful to the environment, but requires special waste management because it is easily flammable according to the Environment Protection Agency (EPA).

## 8.3 Societal Influence

The final design and purpose of this project is for the intended use of our clients lab only. Therefore, the team does not foresee any societal concerns regarding the use or operation of the device. That being said, one potential positive societal impact that this project could have is a role in the advancement and discovery of new and better pharmaceuticals for diseases. The purpose of the device is to aid in the research and advancement of mechanobiology, which in the future could lead to advancements in drug development.

## 8.4 Ethical Concern

The current use and application of the final design does not result in any type of ethical concern. In fact, this device has the potential to decrease the ethical concern regarding the use of *in vivo* animal scaffold models. The improved mechanical properties and cellular characteristics of our engineered tissue scaffolds, in the future have the potential to replace current animal models. This would decrease the need for *in vivo* animal testing during drug development, therefore decrease the ethical concern surrounding drug research.

## 8.5 Health and Safety Issues

The current device does not produce any major type of health or safety concern for the operator, however does have provide a couple minor concerns. The first potential safety issue that the user could run into is by handling the device. Although the device is designed in such a way that the user should not come into contact with the sharp needles often or by accident, it is still important for the operator to maintain vigilance and care when handling the needle plate during setup. The second potential safety concern is in regards to the sterility process. During sterility, the device parts are either autoclave the or put in an 70% ethanol bath. Although, common lab procedure already detail the harmful effect of ethanol it is important to reiterate these practices with consideration to our device. Therefore, the user must use

caution when interacting with ethanol as well as other lab solutions, such as keeping containers closed and practicing appropriate disposal techniques.

# Chapter 9: Conclusion and Recommendations

## 9.1 Conclusions

The actuation system designed and manufactured by our team allows for mechanical stimulation of in vitro tissue scaffolds. Our cam design utilizes a user friendly arduino code which the operator can control the magnitude of strain applied to the scaffold. The compact nature of our design allows for it to be multiplied or even fit into a larger system to allow for higher throughput than eight tissues at a time; this was a long term ambition of our client's which we were able to deliver. Our client did not have a camera or lens that can accurately image the tissue in order to measure and calculate the mechanical properties of the scaffolds. Our team's optic research, system, and designed camera mount allow for the tissue to be captured from both the top and side. Although the device was designed for our clients in the Billiar lab of Worcester Polytechnic Institute, future potential applications of the device include Novartis Institute for BioMedical Research in Cambridge, Massachusetts. Novartis expressed the progressive impact our project could have in the research and development of drugs and treatments for musculoskeletal diseases.

## 9.2 Recommendations

Although the system was successful in meeting the requirements set out by the client, the team believes that there are a few areas which can be further improved to better the ease of use of the device and overall completeness of the device.

One of the main objectives set forth by our client was that the teams device must be highthourghput. The team met this by building a device that actuates an eight well strip at once. While being aware of the clients desire to eventually develop a device that will actuate 96 wells at a time, the team made sure to design a system that can be adapted to a higher throughput. A standard well plate used in the Billiar Labs currently has 96 wells with scaffolds in it. Therefore, it is recommended that multiple identical actuating units be created to actuate many scaffolds at once, then each unit can be exchanged in and out of the imaging space. Our team did a cost analysis of what the total would be to recreate our actuating unit twelve times and actuate all 96 scaffolds at once. The total came to $717.16, which means that one of our actuating units costs only $59.76.

The second recommendation came at the start of the project process, in which the client expressed their interest in electrical stimulation in the system. Our team and client came to the conclusion early on that this was not feasible in our given time frame. That being said, given more time it is recommended that electrical stimulation be incorporated in the future. The team designed the current actuating unit with

the intent of adding electrical rods to the needle plate without much hassle. Two electrical probes could be attached to the needle plate on each side of the needle, creating a electrical field that would travel across the scaffold while in the well. The electrical current could then be turned on and off through the arduino keypad and LCD screen.

A third recommendation that the team believes will improve the device is to incorporate feeding tubes directly to the wells to improve media changing ease of use. Currently, slots in the acrylic top plate allow the user to insert a pipette to change the media, however this is not the most user friendly design. It is important to note that the system currently has no problem with cell culture or media change, however adding this feature to the design would limit the potential for human error and save time for the operator.

The fourth recommendation is also regarding the user-friendliness of the device. The team suggests lengthening the pins in the clear acrylic, such that they stick out of the acrylic plate. This design change will allow the user to grow and seed the scaffolds away from our device in an eight well strip, much like the current process. During loading the pins will be twisted, such that the bent part of the pins are parallel with the scaffolds. When the scaffolds are ready to be actuated and inserted into our device, the user could then easily insert the tissues into the well base without coming in contact or disrupting the pins. Once the well strip is inserted and set in place, the user can use common pliers to twist pins into place, such that they are perpendicularly under the scaffolds and up against the posts. Being able to twist the pins into place will greatly improve the devices ease of use and user compatibility.

Another recommendation came about during the imaging of the actuating unit. The aluminum top piece of the design sometimes interferes with the quality of the picture taken due to the light reflecting off of it and causing glare. Therefore, the team believes that coating the part of aluminum in an anti glare coating. This will not only improve the quality of the picture by eliminating the glare, it will also increase the contrast of the picture, making the scaffolds more visible. Although, this could possible increase the manufacturing cost per actuating unit, if the client were to make multiple units at once it would lower the cost per unit. In addition, the advantage to having more clear and higher quality pictures of the scaffolds, greatly outweigh the slight additional cost.

The sixth recommendation that the team came up with is to machine the cam from aluminum rather than using additive manufacturing. The team is concerned that prolonged use could wear down the 3D printed material causing inaccurate strains on the scaffolds. Therefore, for future and extended use the team suggests machining the part. This aluminum piece does not need to be coated in anti glare material because it is not in the field of view of the images taken and will not interfere with the contrast of the image.

Another recommendation the team has is to purchase higher quality mirrors for side and top view images of the scaffolds. Due to a number of reasons including, price, time and ability to laser cut, the

team had to use lower quality mirrors to prove the concept and functionality of the device and imaging. That being said, the team realized that although the mirror was within our budget and could be laser cut the trade off was the quality of mirror. Therefore, the team suggests that the client invest in higher quality mirrors that will improve the clarity of the side and top view.

The teams last recommendation is to improve the appearance of the devices user interface. In the future the team would like to have a better user set up, where the LCD and keypad were detached from the breadboard to the outside of the box. In addition, a emergency stop button and reset button would be added to the outside of the container to allow the user to restart the program. The other Arduino components would then sit inside the container. This would improve the appearance and professionalism of the user interface and arduino components.

# References


Ahadian, Samad, Serge Ostrovidov, Vahid Hosseini, Hirokazu Kaji, Murugan Ramalingam, Hojae Bae, and Ali Khademhosseini. "Electrical Stimulation as a Biomimicry Tool for Regulating Muscle Cell Behavior." Organogenesis 9, no. 2 (2013): 87-92. doi:10.4161/org.25121.

Akins, Cary W., Mortimer J. Buckley, Willard M. Daggett, Alan D. Hilgenberg, Gus J. Vlahakes, David F. Torchiana, and Joren C. Madsen. "Risk of Reoperative Valve Replacement for Failed Mitral and Aortic Bioprostheses." *The Annals of Thoracic Surgery*65, no. 6 (1998): 1545-552. doi:10.1016/s0003-4975(98)00301-4.

Bursac, N., M. Papadaki, R. J. Cohen, F. J. Schoen, S. R. Eisenberg, R. Carrier, G. Vunjak-Novakovic, and L. E. Freed. "Cardiac Muscle Tissue Engineering: Toward an in Vitro Model for Electrophysiological Studies." American Journal of Physiology-Heart and Circulatory Physiology 277, no. 2 (1999). doi:10.1152/ajpheart.1999.277.2.h433.

Close, R. I. "Dynamic Properties of Mammalian Skeletal Muscles." Physiological Reviews 52, no. 1 (1972): 129-97. doi:10.1152/physrev.1972.52.1.129.

Crystal, Mike. "The Four Properties of Muscle Cells." Sciencing. April 25, 2018. Accessed February 02, 2019. https://sciencing.com/four-properties-muscle-cells-22946.html.

Damore, Antonio, Joao S. Soares, John A. Stella, Will Zhang, Nicholas J. Amoroso, John E. Mayer, William R. Wagner, and Michael S. Sacks. "Large Strain Stimulation Promotes Extracellular Matrix Production and Stiffness in an Elastomeric Scaffold Model." *Journal of the Mechanical Behavior of Biomedical Materials* 62 (2016): 619-35. doi:10.1016/j.jmbbm.2016.05.005.

Das, Mainak, John W. Rumsey, Neelima Bhargava, Maria Stancescu, and James J. Hickman. "Skeletal Muscle Tissue Engineering: A Maturation Model Promoting Long-term Survival of Myotubes, Structural Development of the Excitation–contraction Coupling Apparatus and Neonatal Myosin Heavy Chain Expression." Biomaterials 30, no. 29 (2009): 5392-402. doi:10.1016/j.biomaterials.2009.05.081.

Dennis, Robert G., and Ii Paul E. Kosnik. "Excitability And Isometric Contractile Properties Of Mammalian Skeletal Muscle Constructs Engineered In Vitro." In Vitro Cellular & Developmental Biology - Animal 36, no. 5 (2000): 327. doi:10.1290/1071-2690(2000)0362.0.co;2.

Eisenbarth, E. "Biomaterials for Tissue Engineering." Advanced Engineering Materials 9, no. 12 (2007): 1051-060. doi:10.1002/adem.200700287.

Engelmayr, George C., Daniel K. Hildebrand, Fraser W.h Sutherland, John E. Mayer, and Michael S. Sacks. "A Novel Bioreactor for the Dynamic Flexural Stimulation of Tissue Engineered Heart Valve Biomaterials." Biomaterials 24, no. 14 (2003): 2523-532. doi:10.1016/s0142-9612(03)00051-6.

Ericson, Gwen. "Four out of 106 Heart Replacement Valves from Pig Hearts Failed | The Source | Washington University in St. Louis." The Source. June 29, 2009. Accessed January 06, 2019. https://source.wustl.edu/2009/06/four-out-of-106-heart-replacement-valves-from-pig-hearts-failed/.

Gennisson, Jean-Luc, Thomas Deffieux, Emilie Macé, Gabriel Montaldo, Mathias Fink, and Mickaël Tanter. "Viscoelastic and Anisotropic Mechanical Properties of in Vivo Muscle Tissue Assessed by Supersonic Shear Imaging." Ultrasound in Medicine & Biology 36, no. 5 (2010): 789-801. doi:10.1016/j.ultrasmedbio.2010.02.013.

Grossi, Alberto, Kavita Yadav, and Moira A. Lawson. "Mechanical Stimulation Increases Proliferation, Differentiation and Protein Expression in Culture: Stimulation Effects Are Substrate Dependent." Journal of Biomechanics 40, no. 15 (2007): 3354-362. doi:10.1016/j.jbiomech.2007.05.007.

Hollander, Anthony P., Sally C. Dickinson, Trevor J. Sims, Paola Brun, Roberta Cortivo, Elisaveta Kon, Maurilio Marcacci, Stefano Zanasi, Anna Borrione, Claudio De Luca, Alessandra Pavesio, Carlo Soranzo, and Giovanni Abatangelo. "Maturation of Tissue Engineered Cartilage Implanted in Injured and Osteoarthritic Human Knees." Maturation of Tissue Engineered Cartilage Implanted in Injured and Osteoarthritic Human Knees 12, no. 7 (August 4, 2006) doi:10.1089/ten.2006.12.1787.

Kamble, Harshad, Matthew J. Barton, Myeongjun Jun, Sungsu Park, and Nam-Trung Nguyen. "Cell Stretching Devices as Research Tools: Engineering and Biological Considerations." Lab on a Chip 16, no. 17 (2016): 3193-203. doi:10.1039/c6lc00607h.

Laporte, John. “Topic: Pharmaceutical Industry in the U.S.” Statista, www.statista.com/topics/1719/pharmaceutical-industry/

Madden, Lauran, Mark Juhas, William E. Kraus, George A. Truskey, and Nenad Bursac. "Bioengineered Human Myobundles Mimic Clinical Responses of Skeletal Muscle to Drugs." ELife 4 (2015). doi:10.7554/elife.04885.

Manabe, Yasuko, and Nobuharu L. Fujii. "Experimental Research Models for Skeletal Muscle Contraction." The Journal of Physical Fitness and Sports Medicine 5, no. 5 (2016): 373-77. doi:10.7600/jpfsm.5.373.

Martinez, Ernesto Paredes, Raquel Vargas Jimenez, Atlantida Raya Rivera, and Luis Nino-De-Rivera. "Electrical Stimulation to Vagina Muscle Cells and Rabbit Bladder Muscle and Epithelial Cells In-Vitro to Change Growth Factor." 2009 6th International Conference on Electrical Engineering, Computing Science and Automatic Control (CCE), 2009. doi:10.1109/iceee.2009.5393357.

Merryman, W. David, Howard D. Lukoff, Rebecca A. Long, George C. Engelmayr, Richard A. Hopkins, and Michael S. Sacks. "Synergistic Effects of Cyclic Tension and Transforming Growth Factor-β1 on the Aortic Valve Myofibroblast." Cardiovascular Pathology 16, no. 5 (2007): 268-76. doi:10.1016/j.carpath.2007.03.006.

Moon, Du Geon, George Christ, Joel D. Stitzel, Anthony Atala, and James J. Yoo. "Cyclic Mechanical Preconditioning Improves Engineered Muscle Contraction." Tissue Engineering Part A 14, no. 4 (2008): 473-82. doi:10.1089/tea.2007.0104.

Neuenschwander, Stefan, and Simon P. Hoerstrup. "Heart Valve Tissue Engineering." Transplant Immunology 12, no. 3-4 (2004): 359-65. doi:10.1016/j.trim.2003.12.010.

Nguyen, Nam-Trung, Xiaoyang Huang, and Toh Kok Chuan. "MEMS-Micropumps: A Review." Journal of Fluids Engineering 124, no. 2 (2002): 384. doi:10.1115/1.1459075.

Nikolić, N., S. W. Görgens, G. H. Thoresen, V. Aas, J. Eckel, and K. Eckardt. "Electrical Pulse Stimulation of Cultured Skeletal Muscle Cells as a Model for In vitro Exercise - Possibilities and Limitations." Acta Physiologica 220, no. 3 (2016): 310-31. doi:10.1111/apha.12830.

"NIPAM Based Polymers." Sigma-Aldrich, www.sigmaaldrich.com/materials-science/polymer-science/nipam-polymers.html.

"PDMS: A Review." Elveflow, www.elveflow.com/microfluidic-tutorials/microfluidic-reviews-and-tutorials/the-poly-di-methyl-siloxane-pdms-and-microfluidics/.

Powell, Courtney A., Beth L. Smiley, John Mills, and Herman H. Vandenburgh. "Mechanical Stimulation Improves Tissue-engineered Human Skeletal Muscle." American Journal of Physiology-Cell Physiology 283, no. 5 (2002). doi:10.1152/ajpcell.00595.2001.

Radisic, M., H. Park, H. Shing, T. Consi, F. J. Schoen, R. Langer, L. E. Freed, and G. Vunjak-Novakovic. "Functional Assembly of Engineered Myocardium by Electrical Stimulation of Cardiac Myocytes Cultured on Scaffolds." Proceedings of the National Academy of Sciences 101, no. 52 (2004): 18129-8134. doi:10.1073/pnas.0407817101.

Rangarajan, Swathi, Lauran Madden, and Nenad Bursac. "Use of Flow, Electrical, and Mechanical Stimulation to Promote Engineering of Striated Muscles." Annals of Biomedical Engineering 42, no. 7 (2013): 1391-405. doi:10.1007/s10439-013-0966-4.

Rivera, Luís Ni–O De, Ernesto Paredes Martínez, Daniel Robles Camarillo, and Wilfrido Calleja Arriaga. "Adaptive Electrical Stimulation to Improve In-Vitro Cell Growth." Procedia Technology 3 (2012): 316-23. doi:10.1016/j.protcy.2012.03.034.

Rose, U. "Morphological and Functional Maturation of a Skeletal Muscle Regulated by Juvenile Hormone." Journal of Experimental Biology 207, no. 3 (2004): 483-95. doi:10.1242/jeb.00754.

SEER Training Modules, Structure of Skeletal Muscle. U. S. National Institutes of Health, National Cancer Institute. Available at: https://training.seer.cancer.gov/anatomy/muscular/structure.html

Shimizu, Kazunori, Shigeru Kawakami, Kouji Hayashi, Yuki Mori, Mitsuru Hashida, and Satoshi Konishi. "Implantable Pneumatically Actuated Microsystem for Renal Pressure-mediated Transfection in Mice." Journal of Controlled Release 159, no. 1 (2012): 85-91. doi:10.1016/j.jconrel.2011.12.033.

Stoppel, Whitney L., David L. Kaplan, and Lauren D. Black. "Electrical and Mechanical Stimulation of Cardiac Cells and Tissue Constructs." Advanced Drug Delivery Reviews 96 (2016): 135-55. doi:10.1016/j.addr.2015.07.009.

Tarum, Janelle, Mattias Folkesson, Philip J. Atherton, and Fawzi Kadi. "Electrical Pulse Stimulation: An in Vitro Exercise Model for the Induction of Human Skeletal Muscle Cell Hypertrophy. A Proof-of-concept Study." Experimental Physiology 102, no. 11 (2017): 1405-413. doi:10.1113/ep086581.

Texas Heart Institute. Valve Repair or Replacement. *Texas Heart Institute.* https://www.texasheart.org/heart-health/heart-information-center/topics/valve-repair-or-replacement/

Theadom, Alice, Miriam Rodrigues, Richard Roxburgh, Shiavnthi Balalla, Chris Higgins, Rohit Bhattacharjee, Kelly Jones, Rita Krishnamurthi, and Valery Feigin. "Prevalence of Muscular Dystrophies: A Systematic Literature Review." Neuroepidemiology 43, no. 3-4 (2014): 259-68. doi:10.1159/000369343.

Watanabe, Setsuo, Shuji Inagaki, Ibuki Kinouchi, Hidetada Takai, Yoshinobu Masuda, and Shuichi Mizuno. "Hydrostatic Pressure/perfusion Culture System Designed and Validated for Engineering Tissue." Journal of Bioscience and Bioengineering 100, no. 1 (2005): 105-11. doi:10.1263/jbb.100.105.

Webber, Matthew J., Omar F. Khan, Stefanie A. Sydlik, Benjamin C. Tang, and Robert Langer. "A Perspective on the Clinical Translation of Scaffolds for Tissue Engineering." Annals of Biomedical Engineering 43, no. 3 (2014): 641-56. doi:10.1007/s10439-014-1104-7.

Wells, L., K. A. Edwards, and S. I. Bernstein. "Myosin Heavy Chain Isoforms Regulate Muscle Function but Not Myofibril Assembly." The EMBO Journal 15, no. 17 (1996): 4454-459. doi:10.1002/j.1460-2075.1996.tb00822.x.

Xu, Fan, Ruogang Zhao, Alan S. Liu, Tristin Metz, Yu Shi, Prasenjit Bose, and Daniel H. Reich. "A Microfabricated Magnetic Actuation Device for Mechanical Conditioning of Arrays of 3D Microtissues." Lab on a Chip 15, no. 11 (2015): 2496-503. doi:10.1039/c4lc01395f.

# Appendix A - Arduino Code

**Flow Chart for Arduino Code:**

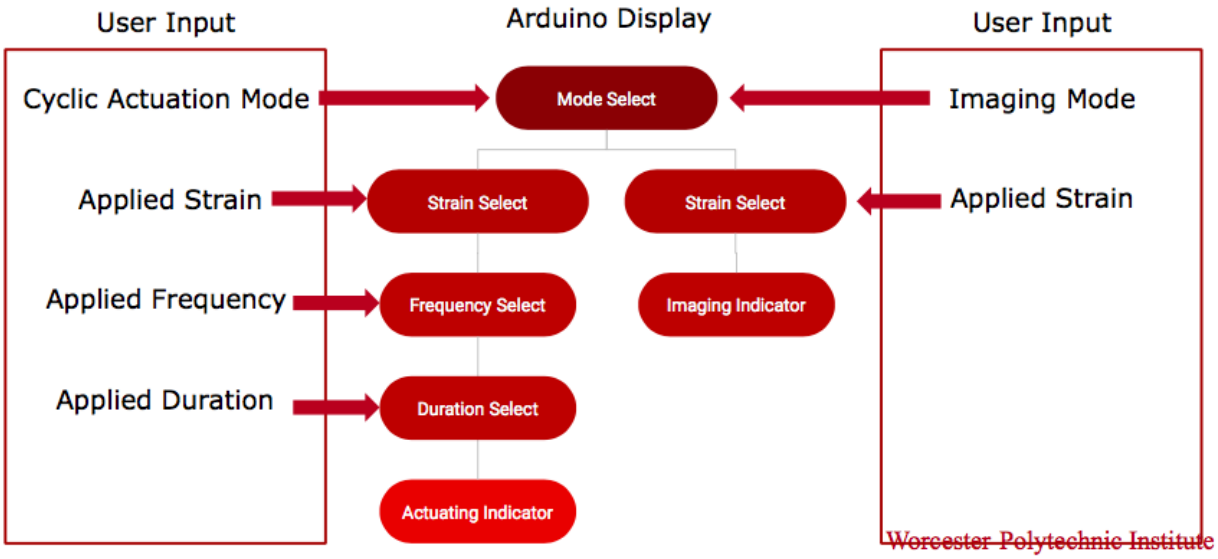


**Wiring Diagram for Arduino Code:**

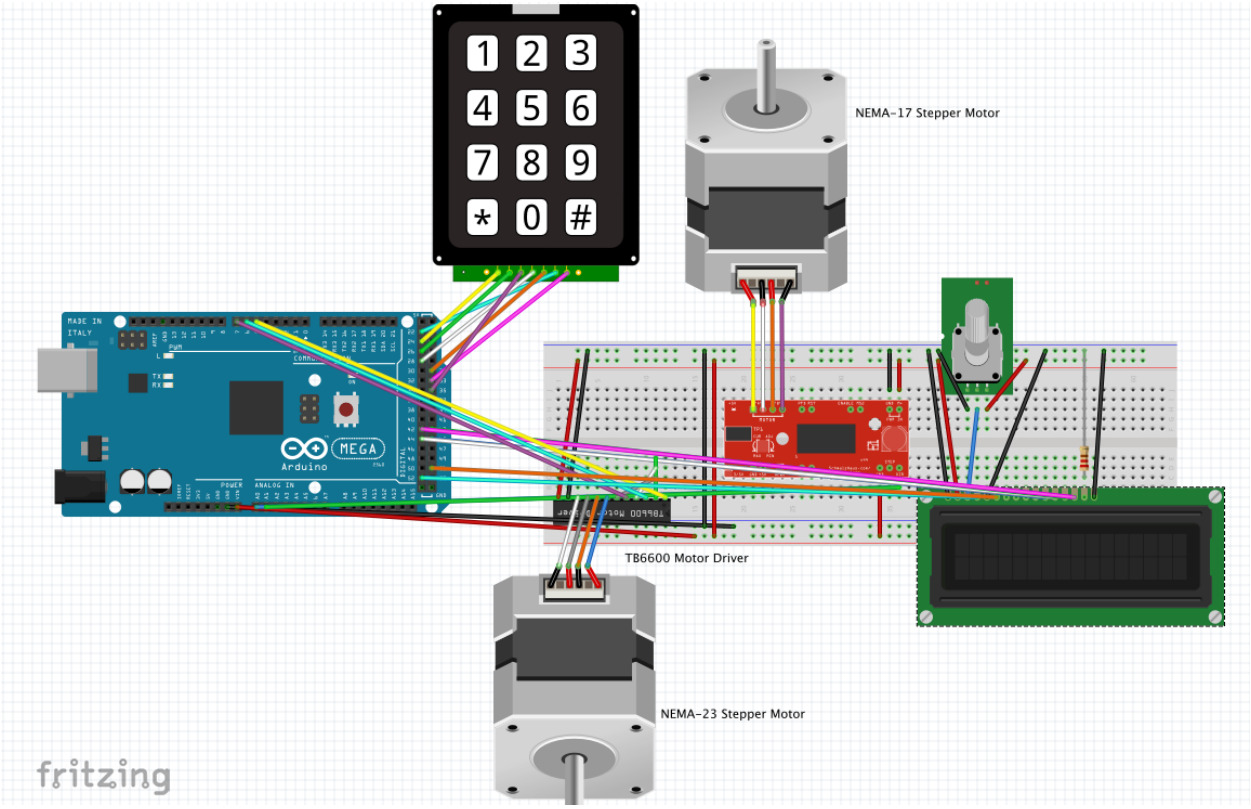

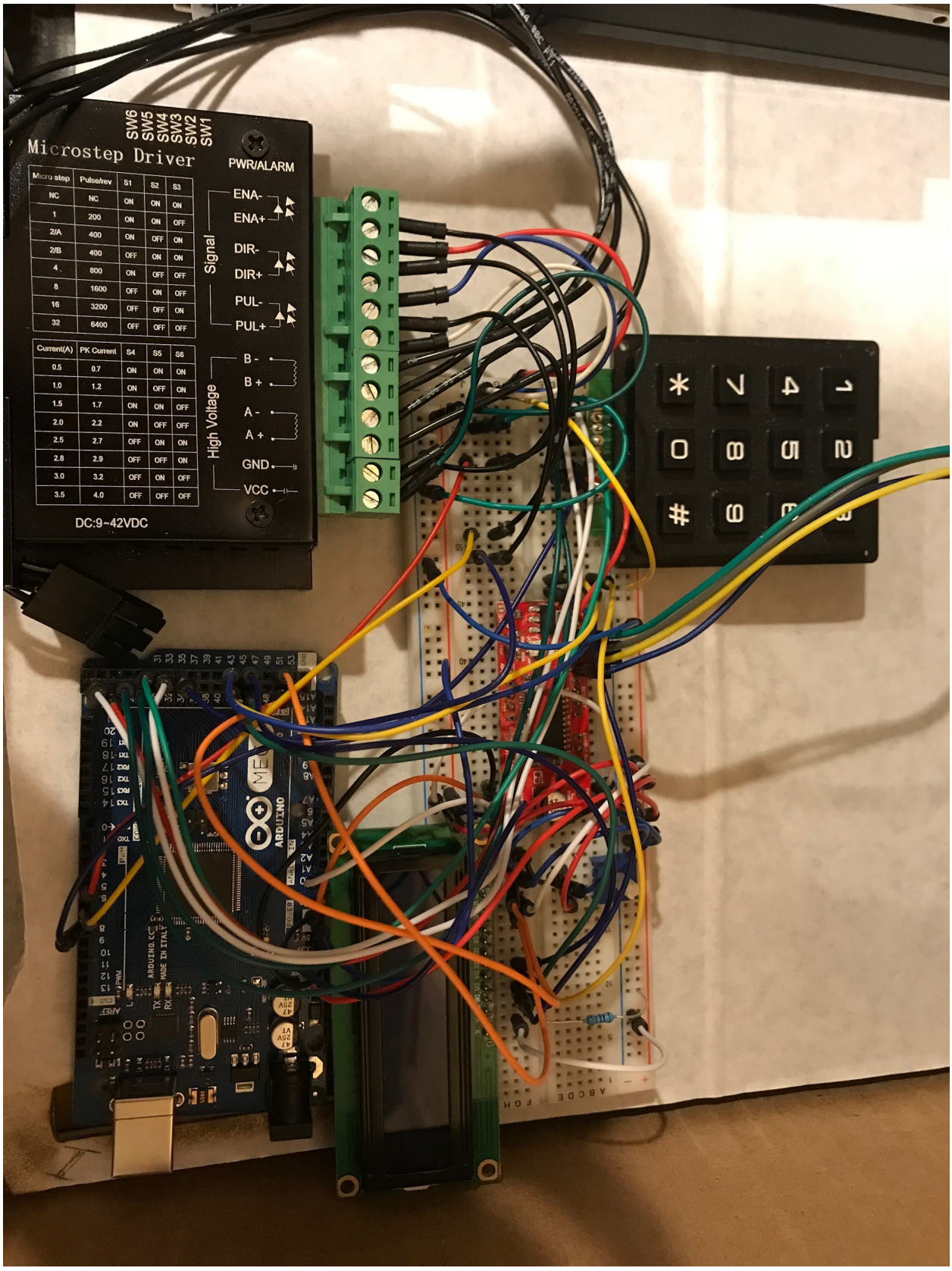
Microstep Driver
SW6 SW5 SW4 SW3 SW2 SW1
PWR/ALARM
Micro step | Pulse/rev | S1 | S2 | S3
NC | NC | ON | ON | ON
1 | 200 | ON | ON | OFF
2/A | 400 | ON | OFF | ON
2/B | 400 | OFF | ON | ON
4 | 800 | ON | OFF | OFF
8 | 1600 | OFF | ON | OFF
16 | 3200 | OFF | OFF | ON
32 | 6400 | OFF | OFF | OFF
Current(A) | PK Current | S4 | S5 | S6
0.5 | 0.7 | ON | ON | ON
1.0 | 1.2 | ON | OFF | ON
1.5 | 1.7 | ON | ON | OFF
2.0 | 2.2 | ON | OFF | OFF
2.5 | 2.7 | OFF | ON | ON
2.8 | 2.9 | OFF | OFF | ON
3.0 | 3.2 | OFF | ON | OFF
3.5 | 4.0 | OFF | OFF | OFF
Signal
ENA-
ENA+
DIR-
DIR+
PUL-
PUL+
High Voltage
B -
B +
A -
A +
GND
VCC
DC:9~42VDC
ARDUINO

**Code for the Arduino:**

```
#include <LiquidCrystal.h> // Include LCD Library
#include <AccelStepper.h>  // AccelStepper Library
#include <Keypad.h>        // Keypad Library
#include <math.h>          // Include math library

// Variables to hold entered number on Keypad
volatile int firstnumber=99;
volatile int secondnumber=99;
volatile int thirdnumber=99;

// Variable to keep track of which mode the screen is in
volatile int modenumber = 1;

// Variables to hold Distance and CurrentPosition
int keyfullnumber=0;  // used to store the final calculated distance value
String currentposition = "";  // Used for display on Nokia LCD

// Variables to hold motor attributes
// In current method, motoracceleration is not used
volatile int motorangle = 0;
volatile int motorspeed = 0;
volatile int motoracceleration = 0;
volatile int motorcycles = 0;

// Keypad Setup
const byte ROWS = 4; // Four Rows
const byte COLS = 3; // Three Columns
char keys[ROWS][COLS] = {
  {'1','2','3'},
  {'4','5','6'},
  {'7','8','9'},
  {'*','0','#'}
};

byte rowPins[ROWS] = {22, 24, 26, 28}; // Arduino pins connected to the row pins of the keypad
byte colPins[COLS] = {31, 33, 35};     // Arduino pins connected to the column pins of the keypad
Keypad keypad = Keypad( makeKeymap(keys), rowPins, colPins, ROWS, COLS );  // Keypad Library
definition

// Initializes LCD display with Arduino pins
const int rs = 52, en = 51, d4 = 45, d5 = 44, d6 = 43, d7 = 42;
LiquidCrystal lcd(rs, en, d4, d5, d6, d7);
```

```
// Cam stepper Setup
AccelStepper stepper1(1, A0, A1);  // 1 = Easy Driver interface
                          // Arduino A0 connected to STEP pin of Easy Driver
                          // Arduino A1 connected to DIR pin of Easy Driver

// Actuator stepper setup
int PUL=7; //define Pulse pin
int DIR=6; //define Direction pin
int ENA=5; //define Enable Pin

void setup(void) {
  // Draw starting screen on LCD
  lcd.begin(16,2);
  lcd.setCursor(0,0);
  lcd.print("Cyclic: 1#");
  lcd.setCursor(0,1);
  lcd.print("Image:  2#");
  pinMode (PUL, OUTPUT);
  pinMode (DIR, OUTPUT);
  pinMode (ENA, OUTPUT);
}

void loop(){
  // Tells Arduino what to do in the case of each number being pressed
  char keypressed = keypad.getKey();  // Get value of keypad button if pressed
  if (keypressed != NO_KEY){  // If keypad button pressed check which key it was
    switch (keypressed) {

      case '1':
        checknumber(1);
      break;

      case '2':
        checknumber(2);
      break;

      case '3':
        checknumber(3);
      break;

      case '4':
        checknumber(4);
      break;
```

```
      case '5':
        checknumber(5);
      break;

      case '6':
        checknumber(6);
      break;

      case '7':
        checknumber(7);
      break;

      case '8':
        checknumber(8);
      break;

      case '9':
        checknumber(9);
      break;

      case '0':
        checknumber(0);
      break;

      case '*':
        deletenumber();
      break;

      case '#':
        checkMode();
      break;
    }
  }
}

void checknumber(int x){
  // Displays the number pressed on the keypad
  if (firstnumber == 99) { // Check if this is the first number entered
    firstnumber=x;
    String displayvalue = String(firstnumber);  //  Transform int to a string for display
    drawnokiascreen(displayvalue, modenumber); // Redraw Nokia lcd

  } else {
```

```
   if (secondnumber == 99) {  // Check if it's the second number entered
     secondnumber=x;
     String displayvalue = (String(firstnumber) + String(secondnumber));
     drawnokiascreen(displayvalue, modenumber);

   } else {
     if (thirdnumber == 99) { //Check that there were only three numbers entered
  thirdnumber=x;
       String displayvalue = (String(firstnumber) + String(secondnumber) + String(thirdnumber));
       drawnokiascreen(displayvalue, modenumber);
     } else {
  //resetnumbers();
  modenumber = modenumber - 1;
  String displayvalue = "";
  drawnokiascreen(displayvalue, modenumber);
  }
}
}
}

void deletenumber() {
  // Used to backspace entered numbers
  if (thirdnumber !=99) {
     String displayvalue = (String(firstnumber) + String(secondnumber));
     drawnokiascreen(displayvalue, modenumber);
    thirdnumber=99;
  }
  else {
    if (secondnumber !=99) {
     String displayvalue = String(firstnumber);
     drawnokiascreen(displayvalue, modenumber);
     secondnumber=99;
   }
   else {
     if (firstnumber !=99) {
      String displayvalue = "";
      drawnokiascreen(displayvalue, modenumber);
      firstnumber=99;
     }
    }
  }
}

void checkMode() {
```

```
// Used to determine which screen the Nokia is on
switch (modenumber) {
  case 1:
     if (thirdnumber == 99 && secondnumber == 99 && firstnumber == 1) {
     drawstrainscreen();
     resetnumbers();
     modenumber = modenumber + 1;
     } else {
       if (thirdnumber == 99 && secondnumber == 99 && firstnumber == 2) {
       drawstrainscreen();
       resetnumbers();
       modenumber = modenumber + 4;
       } else {
         drawmodescreen();
         modenumber = 1;
     }}
  break;
  case 2:
    if (thirdnumber == 99 && secondnumber == 99 && firstnumber != 99) {
    motorangle=firstnumber;
    }
    if (secondnumber != 99 && thirdnumber == 99) {
    motorangle=(firstnumber*10)+secondnumber;
    }
    if (thirdnumber != 99) {
    motorangle=(firstnumber*10)+secondnumber+(thirdnumber*0.1);
    }
    drawfreqscreen();
    resetnumbers();
    modenumber = modenumber + 1;
  break;
  case 3:
    if (thirdnumber == 99 && secondnumber == 99 && firstnumber != 99) {
    motorspeed=firstnumber;
    }
    if (secondnumber != 99 && thirdnumber == 99) {
    motorspeed=firstnumber+(secondnumber*0.1);
    }
    if (thirdnumber != 99) {
    motorspeed=firstnumber+(secondnumber*0.1)+(thirdnumber*0.01);
    }
    drawhourscreen();
    resetnumbers(); // Reset numbers to get ready for new entry
    modenumber = modenumber + 1;
```

```
      break;
      case 4:
        if (thirdnumber == 99 && secondnumber == 99 && firstnumber != 99) {
        motorcycles=firstnumber;
        }
        if (secondnumber != 99 && thirdnumber == 99) {
        motorcycles=(firstnumber*10)+secondnumber;
        }
        if (thirdnumber != 99) {
        motorcycles=(firstnumber*10)+secondnumber+(thirdnumber*0.1);
        }
        drawrunningscreen();
        resetnumbers(); // Reset numbers to get ready for new entry
        movestepper(motorangle, motorspeed, motorcycles);
        modenumber = modenumber + 2;
      break;
      case 5:
        if (thirdnumber == 99 && secondnumber == 99 && firstnumber != 99) {
        motorangle=firstnumber;
        }
        if (secondnumber != 99 && thirdnumber == 99) {
        motorangle=(firstnumber*10)+secondnumber;
        }
        if (thirdnumber != 99) {
        motorangle=(firstnumber*10)+secondnumber+(thirdnumber*0.1);
        }
        drawimagescreen();
        resetnumbers();
        imagestepper(motorangle);
        modenumber = modenumber + 1;
      break;
      case 6:
        resetnumbers();
        drawmodescreen();
        modenumber = 1;
    }
}

void movestepper(int a, int b, int c) {
  //  Moves the stepper using a given motorangle and speed
  if ( a <= 15 && b <= 3 && c <= 24){
    int calculatedmove=((asin(0.125 * (2.2755*a – 2.513) - 1) * 57.296 + 90) * 4.444);  //  Calculate
number of steps needed in mm
    //stepper1.setMaxSpeed(16 * b * (calculatedmove * (360 / 1600) + 100));
```

```
    stepper1.setMaxSpeed(1500);
    //stepper1.setAcceleration(1671);
    stepper1.setAcceleration(calculatedmove * 3.6 * b * b);
    int j = 1;
    int k = (b * 3600 * c);
    while (j < k) {
      stepper1.runToNewPosition(calculatedmove);
      stepper1.runToNewPosition(0);
      j++;
    }
  } else {
    lcd.clear();
    lcd.setCursor(0,0);
    lcd.print("MAX ERROR: 15%,");
    lcd.setCursor(0,1);
    lcd.print("3 Hz, 2 Hrs");
  }
}

void imagestepper(int a) {  //Image the wells
  if ( a <= 15){
    int h = 1;
    while ( h < 8) {
      int calculatedmove=((asin(0.125 * (2.2755*a – 2.513) - 1) * 57.296 + 90) * 4.444);  //  Calculate
number of steps needed in mm
          stepper1.setAcceleration(835);
          stepper1.runToNewPosition(calculatedmove);
          delay(3000);
      stepper1.runToNewPosition(0);
      delay(3000);
      //Code to step actuator 9 mm forward
    for (int i=0; i<27213; i++)    //Forward 5000 steps
    {
      digitalWrite(DIR,LOW);
      digitalWrite(ENA,HIGH);
      digitalWrite(PUL,HIGH);
      delayMicroseconds(50);
      digitalWrite(PUL,LOW);
      delayMicroseconds(50);
    }
      h++;
    }
    //Code to step actuator backwards 63 mm
    for (int i=0; i<190488; i++)   //Backward 5000 steps
```

```
   {
     digitalWrite(DIR,HIGH);
     digitalWrite(ENA,HIGH);
     digitalWrite(PUL,HIGH);
     delayMicroseconds(50);
     digitalWrite(PUL,LOW);
     delayMicroseconds(50);
    }
} else {
   lcd.clear();
   lcd.setCursor(0,0);
   lcd.print("MAX ERROR: 15%");
  }
}

void resetnumbers() {
  // Clears numbers for next entry
  firstnumber=99;
  secondnumber=99;
  thirdnumber=99;
}

void drawnokiascreen(String y, int m) {
// Updates the LCD screen as numbers are being typed in
int z = y.length();
switch(m){
  case 1:
    lcd.setCursor(0,0);
    lcd.print("Cyclic: 1#");
    lcd.setCursor(0,1);
    lcd.print("Image:  2#");
  break;
  case 2:
    lcd.setCursor(0,0);
    lcd.print("Strain:");
    lcd.setCursor(2,1);
    lcd.print(".");
    lcd.setCursor(5,1);
    lcd.print("%");
    switch(z){
      case 1:
        lcd.setCursor(1,1);
        lcd.print(y);
      break;
```

```
    case 2:
      lcd.setCursor(1,1);
      lcd.print(y.charAt(0));
      lcd.setCursor(3,1);
      lcd.print(y.charAt(1));
    break;
    case 3:
      lcd.setCursor(0,1);
      lcd.print(y.charAt(0));
      lcd.setCursor(1,1);
      lcd.print(y.charAt(1));
      lcd.setCursor(3,1);
      lcd.print(y.charAt(2));
    break;
  }
break;
case 3:
  lcd.setCursor(0,0);
  lcd.print("Frequency:");
  lcd.setCursor(1,1);
  lcd.print(".");
  lcd.setCursor(5,1);
  lcd.print("Hz");
  switch(z){
    case 1:
      lcd.setCursor(0,1);
      lcd.print(y);
    break;
    case 2:
      lcd.setCursor(0,1);
      lcd.print(y.charAt(0));
      lcd.setCursor(2,1);
      lcd.print(y.charAt(1));
    break;
    case 3:
      lcd.setCursor(0,1);
      lcd.print(y.charAt(0));
      lcd.setCursor(2,1);
      lcd.print(y.charAt(1));
      lcd.setCursor(3,1);
      lcd.print(y.charAt(2));
    break;
  }
break;
```

```
case 4:
  lcd.setCursor(0,0);
  lcd.print("Hours:");
  lcd.setCursor(2,1);
  lcd.print(".");
  lcd.setCursor(5,1);
  lcd.print("Hrs");
  switch(z){
    case 1:
      lcd.setCursor(1,1);
      lcd.print(y);
    break;
    case 2:
      lcd.setCursor(1,1);
      lcd.print(y.charAt(0));
      lcd.setCursor(3,1);
      lcd.print(y.charAt(1));
    break;
    case 3:
      lcd.setCursor(0,1);
      lcd.print(y.charAt(0));
      lcd.setCursor(1,1);
      lcd.print(y.charAt(1));
      lcd.setCursor(3,1);
      lcd.print(y.charAt(2));
    break;
  }
break;
case 5:
  lcd.setCursor(0,0);
  lcd.print("Strain:");
  lcd.setCursor(2,1);
  lcd.print(".");
  lcd.setCursor(5,1);
  lcd.print("%");
  switch(z){
    case 1:
      lcd.setCursor(1,1);
      lcd.print(y);
    break;
    case 2:
      lcd.setCursor(1,1);
      lcd.print(y.charAt(0));
      lcd.setCursor(3,1);
```

```
      lcd.print(y.charAt(1));
    break;
    case 3:
      lcd.setCursor(0,1);
      lcd.print(y.charAt(0));
      lcd.setCursor(1,1);
      lcd.print(y.charAt(1));
      lcd.setCursor(3,1);
      lcd.print(y.charAt(2));
    break;
   }
 break;
   }
}

void drawstrainscreen() {
    //Draws screen for entering the strain
    lcd.clear();
    lcd.setCursor(0,0);
    lcd.print("Strain:");
    lcd.setCursor(5,1);
    lcd.print("%");

}

void drawfreqscreen() {
    //Draws screen for entering the frequency
    lcd.clear();
    lcd.setCursor(0,0);
    lcd.print("Frequency:");
    lcd.setCursor(5,1);
    lcd.print("Hz");

}

void drawrunningscreen() {
    //Draws screen for when the cam is cyclically running
    lcd.clear();
    lcd.setCursor(0,0);
    lcd.print("Running...");

}

void drawimagescreen() {
```

```
    lcd.clear();
    lcd.setCursor(0,0);
    lcd.print("Imaging wells");
}

void drawmodescreen() {
  //Draws initial mode selection screen
  lcd.clear();
  lcd.setCursor(0,0);
  lcd.print("Cyclic: 1#");
  lcd.setCursor(0,1);
  lcd.print("Image:  2#");

}

void drawhourscreen() {
    //Draws screen for entering the hours
    lcd.clear();
    lcd.setCursor(0,0);
    lcd.print("Hours:");
    lcd.setCursor(5,1);
    lcd.print("Hrs");

}
```

# Appendix B - Cam Equations

When designing the cam for the fixture, an eccentric design was chosen. This allows for easy machining as it is simply a cylinder with an off-center axis. However, this results in a non-linear relationship between the angle about the axis and the radius. In our case, this relationship is the angle the stepper motor moves to and the strain applied respectively. To account for this, the relationship between strain applied to the tissue and angle for the stepper motor to run to was calculated. With these calculations, the team was able to take an entered strain and move the stepper motor and cam to the right angle for the prescribed strain. The equations for the angle of the cam is:

$$Angle = \frac{180°}{\pi} * asin(0.125 * (Strain - 8)) + 90°$$

| | A | B | M | N | O |
|---|---|---|---|---|---|
| 1 | **Offset (mm)** | 1 | | | |
| 2 | **Minimum Radius (mm)** | 12.5 | | | |
| 3 | **Maximum Radius (mm)** | 14.5 | | | |
| 4 | | | | | |
| 5 | **Max Strain** | 16 | | | |
| 6 | | | | | |
| 7 | | | **Equation** | Angle = (180/pi) * asin(0.125 * (Strain - 8)) + 90) | |
| 8 | **Strain** | **Radius** | **Input Strain** | **Output Angle** | |
| 9 | 0 | 12.5 | 0 | 0 | |
| 10 | 0.001 | 12.5125 | 0.5 | 20.36413481 | |
| 11 | 0.002 | 12.525 | 1 | 28.95502437 | |
| 12 | 0.003 | 12.5375 | 1.5 | 35.6590877 | |
| 13 | 0.004 | 12.55 | 2 | 41.40962211 | |
| 14 | 0.005 | 12.5625 | 2.5 | 46.56746344 | |
| 15 | 0.006 | 12.575 | 3 | 51.31781255 | |
| 16 | 0.007 | 12.5875 | 3.5 | 55.77113367 | |
| 17 | 0.008 | 12.6 | 4 | 60 | |
| 18 | 0.009 | 12.6125 | 4.5 | 64.05552023 | |
| 19 | 0.01 | 12.625 | 5 | 67.97568716 | |
| 20 | 0.011 | 12.6375 | 5.5 | 71.79004314 | |
| 21 | 0.012 | 12.65 | 6 | 75.52248781 | |
| 22 | 0.013 | 12.6625 | 6.5 | 79.19307713 | |
| 23 | 0.014 | 12.675 | 7 | 82.81924422 | |
| 24 | 0.015 | 12.6875 | 7.5 | 86.4166783 | |
| 25 | 0.016 | 12.7 | 8 | 90 | |
| 26 | 0.017 | 12.7125 | 8.5 | 93.5833217 | |
| 27 | 0.018 | 12.725 | 9 | 97.18075578 | |
| 28 | 0.019 | 12.7375 | 9.5 | 100.8069229 | |
| 29 | 0.02 | 12.75 | 10 | 104.4775122 | |

# Appendix C - Camera and Lens Specifications

DMK 37BUX178 USB 3.1 Monochrome Industrial Camera Specifications

| General | |
|---|---|
| Vision Standard | USB3 Vision |
| Dynamic Range | 8/12 |
| Resolution | 3072x2048 |
| Frame Rate | 60 |
| Pixel Formats | 8-Bit Monochrome<br>12-Bit Packed Monochrome<br>16-Bit Monochrome |

| Optical Interface | |
|---|---|
| IR-Cut filter | No |
| Sensor Type | Sony IMX178LLJ-C |
| Shutter Type | Rolling |
| Sensor Format | 1/1.8 inch |
| Pixel Size | 2.4 µm |
| Lens Mount | C/CS |

C Series 5MP 16mm 2/3" Fixed Focal Length Imaging Lens Specifications

**55mm Focal Length Partially Telecentric Video Lens**

Stock **#52-271**

| | | | |
|---|---|---|---|
| Primary Magnification PMAG: | 0.5X - 0.4X | Maximum Sensor Format: | 2/3" |
| Aperture (f/#): | f/2.8 - f/32 | Working Distance (mm): | 127 - 158.75 |
| Mount: | C-Mount | Type: | Telecentric Lens |
| Depth of Field (mm): | ±12.5 @ 0.5X | Distortion (%): | <1.0 |
| Field of View, 1/2" Sensor: | Non-Telecentric: 12.8mm - 6.7°<br>Telecentric: 12.8 - 16.0mm | Filter Thread: | M43 x 0.75 |
| Focal Length FL (mm): | 55.0 | Note: | PMAG: Non-Telecentric: 0.5X - 0X<br>Telecentric: 0.5X - 0.4X<br>Working Distance (mm): Non-Telecentric: 127 - ∞<br>Telecentric: 127 - 158.75 |
| Weight (g): | 314.68 | | |

**Regulatory Compliance**

| | | | |
|---|---|---|---|
| Reach 174: | Compliant | RoHS: | Compliant |

# Appendix D: Accuracy Test Data

| | Strained Post | | Stationary Post | | | | |
|---|---|---|---|---|---|---|---|
| | x1 (pixels) | y1 (pixels) | x2 (pixels) | y2 (pixels) | distance (pixels) | strain | % accuracy |
| Home | 1222.000 | 1317.500 | 1231.000 | 502.000 | 815.550 | | |
| 1.1 | 1222.500 | 1327.500 | 1234.000 | 504.000 | 823.580 | 0.985 | 1.531 |
| 1.2 | 1229.000 | 1320.500 | 1237.000 | 496.500 | 824.039 | 1.041 | 4.091 |
| 1.3 | 1228.500 | 1317.000 | 1229.500 | 493.500 | 823.501 | 0.975 | 2.508 |
| 1.4 | 1229.500 | 1317.000 | 1235.500 | 493.500 | 823.522 | 0.978 | 2.248 |
| 1.5 | 1229.000 | 1320.000 | 1233.000 | 496.500 | 823.510 | 0.976 | 2.396 |
| 1.6 | 1226.000 | 1316.000 | 1234.000 | 492.000 | 824.039 | 1.041 | 4.091 |
| 1.7 | 1229.000 | 1319.500 | 1229.500 | 496.500 | 823.000 | 0.914 | 8.645 |
| 1.8 | 1226.000 | 1320.000 | 1229.000 | 496.500 | 823.505 | 0.976 | 2.449 |
| 1.9 | 1228.500 | 1318.500 | 1230.500 | 495.000 | 823.502 | 0.975 | 2.486 |
| 1.10 | 1216.500 | 1321.000 | 1231.000 | 498.000 | 823.128 | 0.929 | 7.080 |
| Average | 1226.450 | 1319.700 | 1232.300 | 496.200 | 823.533 | 0.979 | 3.753 |
| Standard Deviation | | | | | | 0.040 | |
| | | | | | | | |
| | | | | | | | |
| | Strained Post | | Stationary Post | | | | |
| | x1 (pixels) | y1 (pixels) | x2 (pixels) | y2 (pixels) | distance (pixels) | strain | % accuracy |
| Home | 1222.000 | 1317.500 | 1231.000 | 502.000 | 815.550 | | |
| 2.1 | 1157.000 | 1405.000 | 1166.000 | 572.500 | 832.549 | 2.084 | 4.218 |
| 2.2 | 1156.000 | 1396.000 | 1163.000 | 563.000 | 833.029 | 2.143 | 7.165 |
| 2.3 | 1161.000 | 1392.000 | 1170.000 | 559.500 | 832.549 | 2.084 | 4.218 |
| 2.4 | 1158.000 | 1390.500 | 1151.000 | 558.500 | 832.029 | 2.021 | 1.035 |
| 2.5 | 1152.000 | 1393.000 | 1169.000 | 562.000 | 831.174 | 1.916 | 4.211 |
| 2.6 | 1149.000 | 1395.000 | 1176.500 | 563.500 | 831.955 | 2.012 | 0.576 |
| 2.7 | 1159.000 | 1396.500 | 1161.000 | 565.500 | 831.002 | 1.895 | 5.262 |
| 2.8 | 1148.000 | 1398.500 | 1166.500 | 566.000 | 832.706 | 2.104 | 5.180 |

| | | | | | | | |
|---|---|---|---|---|---|---|---|
| 2.9 | 1158.000 | 1395.500 | 1167.000 | 564.500 | 831.049 | 1.900 | 4.978 |
| 2.10 | 1144.000 | 1397.500 | 1156.000 | 565.500 | 832.087 | 2.028 | 1.385 |
| Average | 1154.200 | 1395.950 | 1164.600 | 564.050 | 832.013 | 2.019 | 3.823 |
| Standard Deviation | | | | | | 0.089 | |
| | | | | | | | |
| | | | | | | | |
| | Strained Post | | Stationary Post | | | | |
| | x1 (pixels) | y1 (pixels) | x2 (pixels) | y2 (pixels) | distance (pixels) | strain | % accuracy |
| Home | 1222.000 | 1317.500 | 1231.000 | 502.000 | 815.550 | | |
| 3.1 | 1159.000 | 1393.500 | 1180.500 | 554.000 | 839.775 | 2.970 | 0.985 |
| 3.2 | 1169.500 | 1389.500 | 1180.500 | 550.500 | 839.072 | 2.884 | 3.859 |
| 3.3 | 1163.000 | 1386.000 | 1177.500 | 547.500 | 838.625 | 2.829 | 5.684 |
| 3.4 | 1162.500 | 1390.500 | 1173.500 | 550.500 | 840.072 | 3.007 | 0.228 |
| 3.5 | 1163.500 | 1392.000 | 1177.500 | 552.000 | 840.117 | 3.012 | 0.411 |
| 3.6 | 1162.500 | 1392.500 | 1175.500 | 553.500 | 839.101 | 2.888 | 3.742 |
| 3.7 | 1161.500 | 1390.000 | 1174.500 | 550.000 | 840.101 | 3.010 | 0.345 |
| 3.8 | 1156.500 | 1390.500 | 1177.500 | 552.000 | 838.763 | 2.846 | 5.122 |
| 3.9 | 1161.000 | 1392.000 | 1173.000 | 552.000 | 840.086 | 3.009 | 0.284 |
| 3.10 | 1160.000 | 1390.500 | 1174.500 | 550.500 | 840.125 | 3.013 | 0.445 |
| Average | 1161.900 | 1390.700 | 1176.450 | 551.250 | 839.584 | 2.947 | 2.111 |
| Standard Deviation | | | | | | 0.076 | |
| | | | | | | | |
| | | | | | | | |
| | Strained Post | | Stationary Post | | | | |
| | x1 (pixels) | y1 (pixels) | x2 (pixels) | y2 (pixels) | distance (pixels) | strain | % accuracy |
| Home | 1222.000 | 1317.500 | 1231.000 | 502.000 | 815.550 | | |
| 4.1 | 1175.000 | 1401.500 | 1192.500 | 552.000 | 849.680 | 4.185 | 4.624 |
| 4.2 | 1172.000 | 1396.500 | 1185.500 | 549.000 | 847.608 | 3.931 | 1.729 |
| 4.3 | 1176.000 | 1390.500 | 1186.500 | 543.500 | 847.065 | 3.864 | 3.392 |
| 4.4 | 1178.000 | 1389.000 | 1183.500 | 541.500 | 847.518 | 3.920 | 2.004 |

| | | | | | | | |
|---|---|---|---|---|---|---|---|
| 4.5 | 1175.000 | 1389.000 | 1184.500 | 542.500 | 846.553 | 3.802 | 4.961 |
| 4.6 | 1179.000 | 1401.000 | 1181.000 | 553.000 | 848.002 | 3.979 | 0.519 |
| 4.7 | 1175.000 | 1403.500 | 1180.500 | 555.000 | 848.518 | 4.042 | 1.061 |
| 4.8 | 1181.500 | 1402.500 | 1185.500 | 555.000 | 847.509 | 3.919 | 2.030 |
| 4.9 | 1177.500 | 1400.000 | 1187.000 | 552.500 | 847.553 | 3.924 | 1.896 |
| 4.10 | 1179.000 | 1395.000 | 1186.000 | 547.000 | 848.029 | 3.982 | 0.438 |
| Average | 1176.800 | 1396.850 | 1185.250 | 549.100 | 847.804 | 3.955 | 2.265 |
| Standard Deviation | | | | | | 0.104 | |
| | | | | | | | |
| | | | | | | | |
| | Strained Post | | Stationary Post | | | | |
| | x1 (pixels) | y1 (pixels) | x2 (pixels) | y2 (pixels) | distance (pixels) | strain | % accuracy |
| Home | 1222.000 | 1317.500 | 1231.000 | 502.000 | 815.550 | | |
| 5.1 | 1234.000 | 1359.000 | 1239.000 | 502.500 | 856.515 | 5.023 | 0.460 |
| 5.2 | 1232.500 | 1359.000 | 1235.500 | 501.000 | 858.005 | 5.206 | 4.115 |
| 5.3 | 1231.000 | 1353.000 | 1236.500 | 497.000 | 856.018 | 4.962 | 0.759 |
| 5.4 | 1232.500 | 1354.500 | 1238.500 | 499.000 | 855.521 | 4.901 | 1.977 |
| 5.5 | 1230.500 | 1357.500 | 1237.000 | 500.500 | 857.025 | 5.086 | 1.711 |
| 5.6 | 1230.000 | 1356.000 | 1239.500 | 501.000 | 855.053 | 4.844 | 3.125 |
| 5.7 | 1229.000 | 1358.500 | 1237.000 | 500.500 | 858.037 | 5.210 | 4.194 |
| 5.8 | 1232.500 | 1351.500 | 1236.500 | 496.000 | 855.509 | 4.900 | 2.006 |
| 5.9 | 1231.000 | 1356.000 | 1235.500 | 501.000 | 855.012 | 4.839 | 3.226 |
| 5.10 | 1232.500 | 1352.000 | 1234.500 | 496.500 | 855.502 | 4.899 | 2.023 |
| Average | 1231.550 | 1355.700 | 1236.950 | 499.500 | 856.220 | 4.987 | 2.359 |
| Standard Deviation | | | | | | 0.139 | |
| | | | | | | | |
| | | | | | | | |
| | Strained Post | | Stationary Post | | | | |
| | x1 (pixels) | y1 (pixels) | x2 (pixels) | y2 (pixels) | distance (pixels) | strain | % accuracy |
| Home | 1222.000 | 1317.500 | 1231.000 | 502.000 | 815.550 | | |

| | | | | | | | |
|---|---|---|---|---|---|---|---|
| 6.1 | 1236.000 | 1357.500 | 1242.500 | 493.000 | 864.524 | 6.005 | 0.085 |
| 6.2 | 1230.000 | 1355.000 | 1243.500 | 492.000 | 863.106 | 5.831 | 2.814 |
| 6.3 | 1228.000 | 1346.000 | 1245.500 | 483.500 | 862.678 | 5.779 | 3.689 |
| 6.4 | 1230.000 | 1350.000 | 1243.500 | 484.500 | 865.605 | 6.138 | 2.294 |
| 6.5 | 1227.500 | 1344.500 | 1249.000 | 483.500 | 861.268 | 5.606 | 6.569 |
| 6.6 | 1234.000 | 1351.000 | 1250.000 | 488.500 | 862.648 | 5.775 | 3.748 |
| 6.7 | 1229.500 | 1348.500 | 1251.500 | 483.000 | 865.780 | 6.159 | 2.650 |
| 6.8 | 1225.000 | 1347.000 | 1241.000 | 486.000 | 861.149 | 5.591 | 6.813 |
| 6.9 | 1221.000 | 1352.000 | 1246.500 | 487.500 | 864.876 | 6.048 | 0.804 |
| 6.10 | 1233.500 | 1349.000 | 1265.500 | 485.000 | 864.592 | 6.013 | 0.224 |
| Average | 1229.450 | 1350.050 | 1247.850 | 486.650 | 863.623 | 5.895 | 2.969 |
| Standard Deviation | | | | | | 0.207 | |
| | | | | | | | |
| | | | | | | | |
| | Strained Post | | Stationary Post | | | | |
| | x1 (pixels) | y1 (pixels) | x2 (pixels) | y2 (pixels) | distance (pixels) | strain | % accuracy |
| Home | 1222.000 | 1317.500 | 1231.000 | 502.000 | 815.550 | | |
| 7.1 | 1237.500 | 1350.500 | 1259.500 | 478.000 | 872.777 | 7.017 | 0.244 |
| 7.2 | 1239.000 | 1342.000 | 1263.500 | 474.000 | 868.346 | 6.474 | 7.519 |
| 7.3 | 1239.000 | 1345.500 | 1246.600 | 472.500 | 873.033 | 7.048 | 0.692 |
| 7.4 | 1237.000 | 1352.500 | 1258.000 | 478.000 | 874.752 | 7.259 | 3.703 |
| 7.5 | 1243.000 | 1349.000 | 1258.500 | 475.000 | 874.137 | 7.184 | 2.626 |
| 7.6 | 1239.000 | 1349.500 | 1260.000 | 476.500 | 873.253 | 7.075 | 1.076 |
| 7.7 | 1235.500 | 1348.500 | 1251.500 | 475.000 | 873.647 | 7.124 | 1.766 |
| 7.8 | 1239.000 | 1347.500 | 1272.500 | 473.000 | 875.141 | 7.307 | 4.385 |
| 7.9 | 1235.000 | 1344.500 | 1274.000 | 472.500 | 872.872 | 7.029 | 0.409 |
| 7.10 | 1241.500 | 1349.000 | 1262.000 | 476.500 | 872.741 | 7.013 | 0.180 |
| Average | 1238.550 | 1347.850 | 1260.610 | 475.100 | 873.070 | 7.053 | 2.260 |
| Standard Deviation | | | | | | 0.228 | |
| | | | | | | | |
| | | | | | | | |

| | Strained Post | | Stationary Post | | | | |
|---|---|---|---|---|---|---|---|
| | x1 (pixels) | y1 (pixels) | x2 (pixels) | y2 (pixels) | distance (pixels) | strain | % accuracy |
| Home | 1222.000 | 1317.500 | 1231.000 | 502.000 | 815.550 | | |
| 8.1 | 1229.000 | 1359.000 | 1249.000 | 478.500 | 880.727 | 7.992 | 0.102 |
| 8.2 | 1233.500 | 1349.000 | 1253.000 | 472.000 | 877.217 | 7.561 | 5.482 |
| 8.3 | 1234.000 | 1355.500 | 1255.000 | 474.500 | 881.250 | 8.056 | 0.700 |
| 8.4 | 1235.000 | 1356.000 | 1255.500 | 474.000 | 882.238 | 8.177 | 2.214 |
| 8.5 | 1232.500 | 1356.000 | 1254.500 | 474.500 | 881.774 | 8.120 | 1.503 |
| 8.6 | 1235.000 | 1359.500 | 1260.500 | 473.000 | 886.867 | 8.745 | 9.308 |
| 8.7 | 1233.500 | 1358.000 | 1251.000 | 472.500 | 885.673 | 8.598 | 7.479 |
| 8.8 | 1239.000 | 1354.500 | 1254.000 | 473.500 | 881.128 | 8.041 | 0.512 |
| 8.9 | 1232.500 | 1359.500 | 1255.000 | 475.500 | 884.286 | 8.428 | 5.353 |
| 8.10 | 1234.000 | 1351.500 | 1257.000 | 472.500 | 879.301 | 7.817 | 2.288 |
| Average | 1233.800 | 1355.850 | 1254.450 | 474.050 | 882.046 | 8.154 | 3.494 |
| Standard Deviation | | | | | | 0.355 | |
| | | | | | | | |
| | | | | | | | |
| | Strained Post | | Stationary Post | | | | |
| | x1 (pixels) | y1 (pixels) | x2 (pixels) | y2 (pixels) | distance (pixels) | strain | % accuracy |
| Home | 1222.000 | 1317.500 | 1231.000 | 502.000 | 815.550 | | |
| 9.1 | 1234.500 | 1359.000 | 1259.500 | 470.500 | 888.852 | 8.988 | 0.133 |
| 9.2 | 1237.500 | 1362.000 | 1250.000 | 475.000 | 887.088 | 8.772 | 2.536 |
| 9.3 | 1239.500 | 1358.000 | 1257.500 | 467.000 | 891.182 | 9.274 | 3.042 |
| 9.4 | 1238.000 | 1357.500 | 1252.500 | 472.000 | 885.619 | 8.592 | 4.537 |
| 9.5 | 1236.000 | 1357.500 | 1257.000 | 471.500 | 886.249 | 8.669 | 3.679 |
| 9.6 | 1246.000 | 1356.000 | 1252.000 | 469.000 | 887.020 | 8.763 | 2.628 |
| 9.7 | 1242.000 | 1356.000 | 1247.500 | 470.500 | 885.517 | 8.579 | 4.676 |
| 9.8 | 1241.500 | 1357.500 | 1253.000 | 471.500 | 886.075 | 8.648 | 3.916 |
| 9.9 | 1249.500 | 1357.500 | 1249.000 | 471.500 | 886.000 | 8.638 | 4.018 |
| 9.10 | 1241.000 | 1357.000 | 1249.000 | 470.000 | 887.036 | 8.765 | 2.606 |

| | | | | | | | |
|---|---|---|---|---|---|---|---|
| Average | 1240.550 | 1357.800 | 1252.700 | 470.850 | 887.064 | 8.769 | 3.177 |
| Standard Deviation | | | | | | 0.214 | |
| | | | | | | | |
| | | | | | | | |
| | Strained Post | | Stationary Post | | | | |
| | x1 (pixels) | y1 (pixels) | x2 (pixels) | y2 (pixels) | distance (pixels) | strain | % accuracy |
| Home | 1222.000 | 1317.500 | 1231.000 | 502.000 | 815.550 | | |
| 10.1 | 1255.000 | 1362.000 | 1266.000 | 465.000 | 897.067 | 9.995 | 0.046 |
| 10.2 | 1254.500 | 1359.500 | 1259.500 | 463.500 | 896.014 | 9.866 | 1.337 |
| 10.3 | 1253.500 | 1361.000 | 1256.500 | 467.000 | 894.005 | 9.620 | 3.801 |
| 10.4 | 1253.500 | 1364.500 | 1256.500 | 467.000 | 897.505 | 10.049 | 0.491 |
| 10.5 | 1252.000 | 1363.000 | 1255.000 | 466.500 | 896.505 | 9.926 | 0.735 |
| 10.6 | 1253.000 | 1363.500 | 1255.500 | 464.000 | 899.503 | 10.294 | 2.941 |
| 10.7 | 1252.000 | 1361.000 | 1260.500 | 467.000 | 894.040 | 9.624 | 3.757 |
| 10.8 | 1253.000 | 1366.000 | 1256.500 | 471.000 | 895.007 | 9.743 | 2.572 |
| 10.9 | 1253.000 | 1364.500 | 1256.500 | 469.000 | 895.507 | 9.804 | 1.959 |
| 10.10 | 1251.000 | 1363.500 | 1253.500 | 469.500 | 894.003 | 9.620 | 3.803 |
| Average | 1253.050 | 1362.850 | 1257.600 | 466.950 | 895.916 | 9.854 | 2.144 |
| Standard Deviation | | | | | | 0.220 | |

# Appendix E - Refraction Calculations for Curvature of Wells

Refraction calculations were performed using the diagram below. N1 represents the refraction index of air. N2 is the refraction index of the polycarbonate well. Finally n3 represents the refraction index of the media because the media is made from 93% water, the refraction index of water was used to perform the calculations. Using the equation shown in the diagram, refraction calculations signifying the observed distance to the actual distance of the posts in the wells were completed. The results are shown in the chart below. The rows highlighted in red are outside of the working range of the strains desired. While the rows in green represent strains and deflections distances that the client will use.

| | |
|---|---|
| n1 | 1.00029 |
| n2 | 1.60 |
| n3 | 1.33 |

| Theta 1 | X i | Theta 2 | Theta 5 | Theta 3 | Theta 4 | X f | Delta X (mm) |
|---|---|---|---|---|---|---|---|
| 180 | -4.21 | 38.70 | 14.20 | 52.90 | 73.64 | -3.68 | 0.53 |
| 170 | -4.15 | 38.00 | 13.76 | 51.76 | 70.89 | -3.38 | 0.76 |
| 160 | -3.96 | 35.98 | 12.57 | 48.55 | 64.37 | -3.13 | 0.82 |
| 150 | -3.65 | 32.78 | 10.91 | 43.69 | 56.20 | -2.84 | 0.81 |
| 140 | -3.23 | 28.61 | 9.05 | 37.66 | 47.31 | -2.48 | 0.75 |
| 130 | -2.71 | 23.69 | 7.15 | 30.84 | 38.08 | -2.06 | 0.65 |
| 120 | -2.11 | 18.22 | 5.29 | 23.50 | 28.67 | -1.59 | 0.51 |
| 110 | -1.44 | 12.35 | 3.48 | 15.83 | 19.16 | -1.09 | 0.35 |
| 100 | -0.73 | 6.23 | 1.73 | 7.96 | 9.59 | -0.55 | 0.18 |
| 90 | 0.00 | 0.00 | 0.00 | 0.00 | 0.00 | 0.00 | 0.00 |
| 80 | 0.73 | 6.23 | 1.73 | 7.96 | 9.59 | 0.55 | 0.18 |
| 70 | 1.44 | 12.35 | 3.48 | 15.83 | 19.16 | 1.09 | 0.35 |
| 60 | 2.11 | 18.22 | 5.29 | 23.50 | 28.67 | 1.59 | 0.51 |
| 50 | 2.71 | 23.69 | 7.15 | 30.84 | 38.08 | 2.06 | 0.65 |
| 40 | 3.23 | 28.61 | 9.05 | 37.66 | 47.31 | 2.48 | 0.75 |
| 30 | 3.65 | 32.78 | 10.91 | 43.69 | 56.20 | 2.84 | 0.81 |
| 20 | 3.96 | 35.98 | 12.57 | 48.55 | 64.37 | 3.13 | 0.82 |
| 10 | 4.15 | 38.00 | 13.76 | 51.76 | 70.89 | 3.38 | 0.76 |

| | | | | | | | |
|---|---|---|---|---|---|---|---|
| 0 | 4.21 | 38.70 | 14.20 | 52.90 | 73.64 | 3.68 | 0.53 |

# Appendix F - Copyright Approval for Figures

All figures were contacted either through email or through their respective copyright websites, such as Copyright Clearance Center to obtain copyright approval for use in an academic paper. Although all figures were contacted only four places responded after repeated attempts. Pictures that did not require copyright approval were taken or created by the group and therefore don't need copyright approval.

| Figure number | Approval |
|---|---|
| Figure 1: Muscle Anatomy | Yes |
| Figure 2: Growth Process of Muscle Tissue | Yes |
| Figure 3: Determining Degree of Muscle Fiber Alignment | Yes |
| Figure 4: Mechanical Actuation by Bioreactor Step Motor System | Yes |
| Figure 5: Mechanical Actuation by Linear Actuator | Yes |
| Figure 6: Pneumatic Stimulation of Cells | Yes |
| Figure 7: Magnetic Actuation of Microtissues | Yes |
| Figure 8: Electrical Stimulation of Muscle Cells Using Stainless Steel Electrodes | Yes |

# Copyright

This page has information about general copyright restrictions that apply to the material that is available through the Europe PMC site. There are also links to some Publisher Specific Copyright Information.

All of the material available through the Europe PMC site is provided by the respective publishers or authors. Almost all of it is protected by U.K. and/or foreign copyright laws, even though Europe PMC provides free access to it (See Public Domain Material below, for exceptions).

The respective copyright holders retain rights for reproduction, redistribution and reuse. Users of Europe PMC are directly and solely responsible for compliance with copyright restrictions and are expected to adhere to the terms and conditions defined by the copyright holder. Transmission, reproduction, or reuse of protected material, beyond that allowed by the fair use principles of the copyright laws, requires the written permission of the copyright owners.

## Order Completed

Thank you for your order.

This Agreement between 100 Institute Rd PO 1966 ("You") and Elsevier ("Elsevier") consists of your license details and the terms and conditions provided by Elsevier and Copyright Clearance Center.

Your confirmation email will contain your order number for future reference.

printable details

| | |
|---|---|
| License Number | 4536771361840 |
| License date | Feb 26, 2019 |
| Licensed Content Publisher | Elsevier |
| Licensed Content Publication | Cardiovascular Pathology |
| Licensed Content Title | Synergistic effects of cyclic tension and transforming growth factor-β1 on the aortic valve myofibroblast |
| Licensed Content Author | W. David Merryman,Howard D. Lukoff,Rebecca A. Long,George C. Engelmayr,Richard A. Hopkins,Michael S. Sacks |
| Licensed Content Date | September–October 2007 |
| Licensed Content Volume | 16 |
| Licensed Content Issue | 5 |
| Licensed Content Pages | 9 |
| Type of Use | reuse in coursepack/classroom materials |
| Requestor type | academic/educational institute |

| | |
|---|---|
| My billing country | US |
| Intended publisher of new work | Open University |
| Other institution name | Open University |
| Portion | figures/tables/illustrations |
| Number of figures/tables/illustrations | 1 |
| Number of students | 4 |
| Format | electronic |
| Are you the author of this Elsevier article? | Yes |
| Will you be translating? | No |
| Original figure numbers | Figure 2 |
| Course name | Major Qualifying Project |

[redacted]

| | |
|---|---|
| Institution name | Open University |
| Instructor name | Kristen Billiar |
| Expected course start date | Jun 2019 |
| Course end date | May 2019 |
| Requestor Location | 100 Institute Rd PO 1966<br>100 Institute Rd<br>PO Box 1966<br><br>WORCESTER, MA 01609<br>United States<br>Attn: 100 Institute Rd PO 1966 |
| Publisher Tax ID | 98-0397604 |
| Total | 0.00 USD |


## Thank you for your order!

Dear Mrs. Katherine Kowalczyk,

Thank you for placing your order through Copyright Clearance Center's RightsLink® service.

**Order Summary**

| | |
|---|---|
| Licensee: | Mrs. Katherine Kowalczyk |
| Order Date: | Feb 27, 2019 |
| Order Number: | 4537171100791 |
| Publication: | IEEE Proceedings |
| Title: | Electrical stimulation to vagina muscle cells and rabbit bladder muscle and epithelial cells In-Vitro to change growth factor |
| Type of Use: | Report |
| Order Total: | 0.00 USD |

View or print complete details of your order and the publisher's terms and conditions.

Sincerely,

Copyright Clearance Center

N

NCI DCCPS SEER Training Website <SEERTrainingSite@mail.nih.gov>

Wed 2/27/2019 11:02 AM

Velashea, Victoria Tianyu

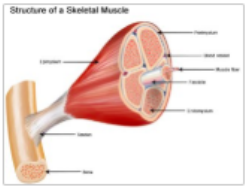


Hi Vicky,

That should be fine to use the attached muscle figure. If so, please credit the: National Cancer Institute of the National Institutes of Health, Department of Health and Human Services of the United States Government. Many thanks.

Alison

**Alison L. Van Dyke, MD, PhD**
Physician
Data Quality, Analysis, and Interpretation Branch
Surveillance Research Program
Division of Cancer Control and Population Sciences
National Cancer Institute
National Institutes of Health
9609 Medical Center Drive, 4E348
Rockville, MD 20850
Phone: 240-276-6039
Fax: 240-276-7908
Email: alison.vandyke@nih.gov

# Appendix G - Cost Analysis of Device

| Object | Price | Link |
|---|---|---|
| **Actuating Unit** | | |
| NEMA 17 Motor | 14 | https://www.digikey.com/product-detail/en/adafruit-industries-llc/324/1528-1062-ND/5022791 |
| 3D Printed Parts | 1.61 | from Fosie Innovation Studio |
| Aluminum Part | 7.72 | https://www.mcmaster.com/8975k59 |
| Screws (M3) | 4.72 | https://www.mcmaster.com/91292a113 |
| Screw Inserts (M3) | 16.15 | https://www.mcmaster.com/94180a333 |
| Spring | 10.36 | https://www.mcmaster.com/94125k412 |
| Acrylic for Top Plate & Sides | 8.06 | https://www.mcmaster.com/8589k61 |
| Acrylic for Cover | 4.67 | https://www.mcmaster.com/8589k11 |
| Needles | 3.99 | https://www.michaels.com/dritz--1.25in-dressmaker-pins--350-count/D082385S.html#q=pin&prefn1=size&pmpt=qualifying&prefv1=1.25%20in&start=3 |
| Mirror | 15.28 | https://www.mcmaster.com/8344t51 |
| **Arduino Parts** | | |
| Arduino Mega | 38.5 | https://store.arduino.cc/usa/mega-2560-r3 |
| Keypad | 6.5 | https://www.adafruit.com/product/3845 |
| Nokia Screen | 10 | https://www.adafruit.com/product/338 |
| Wires | 7.29 | https://www.amazon.com/Solderless-Flexible-Breadboard-Jumper-100pcs/dp/B005TZJ0AM/ref=sr_1_5?crid=3N2NCSXHKHFPB&keywords=breadboard+jumper+wires&qid=1555525775&s=industrial&sprefix=breadboard%2Cindustrial%2C128&sr=1-5 |
| Motor Driver for 23 | 14.9 | https://www.amazon.com/SMAKN-Upgraded-Version-Segments-Stepper/dp/B016ZJS1FA |
| Motor Driver for 17 | 9.69 | https://www.amazon.com/CJRSLRB-EasyDriver-Stepper-Headers-Arduino/dp/B07BJXCNS8/ref=sr_1_1_sspa?keywords=easy+driver&qid=1555525886&s=industrial&sr=1-1-spons&psc=1 |
| Breadboard | 9.99 | https://www.amazon.com/Breadboards-Solderless-Breadboard-Distribution-Connecting/dp/B07DL13RZH/ref=pd_day0_hl_60_1/183 |

| | | |
|---|---|---|
| | | -5376490-1961429?_encoding=UTF8&pd_rd_i=B07DL13RZH&pd_rd_r=47825156-613e-11e9-b2ef-bb2ae37525d6&pd_rd_w=xetQp&pd_rd_wg=XAFZO&pf_rd_p=ad07871c-e646-4161-82c7-5ed0d4c85b07&pf_rd_r=0YC65T97YQHG3H5251G8&psc=1&refRID=0YC65T97YQHG3H5251G8 |
| Voltage Source | 58.93 | https://power.sager.com/pmp60-12-3978786.html |
| **Imaging Actuator** | | |
| NEMA Motor 23 | 26 | https://www.amazon.com/gp/product/B00PNEPF5I/ref=ppx_yo_dt_b_asin_title_o03_s00?ie=UTF8&psc=1 |
| Linear Actuator | 165 | https://www.ebay.com/itm/THK-KR26-Linear-Ball-Screw-Actuator-70mm-Travel-NEMA-23-W-Shaft-Coupling/401554898762?epid=26020596599&hash=item5d7e897f4a:g:7ecAAOSwVK9bKV9S:sc:USPSPriorityMailPaddedFlatRateEnvelope!01609!US!-1:rk:19:pf:0 |
| Motor Coupler | 46.13 | https://www.mcmaster.com/2464k17 |
| 3D Printed Parts | 1.61 | from Fosie Innovation Studio |
| **Camera, Lens and Camera Mount** | | |
| Camera | 500 | https://www.theimagingsource.com/products/industrial-cameras/usb-3.1-monochrome/dmk37bux178/ |
| Lens | 595 | https://www.edmundoptics.com/f/55mm-FL-Partially-Telecentric-Imaging-Lens/12332/ |
| 8020 | 24.43 | https://www.mcmaster.com/47065t108 |
| 3D Printed Parts | 4.22 | from Fosie Innovation Studio |
| Screws for Base (5/16"-18) | 9.42 | https://www.mcmaster.com/92196a580 |
| Screw Inserts | 13.06 | https://www.mcmaster.com/93365a270 |
| Screws for Camera (M3) | 5.75 | https://www.mcmaster.com/92855a307 |
| | | |
| **Total Price** | **1632.98** | |